FIGURES

FIGURE 1: The externally visible anatomy and body weight of adult zebrafish are not affected by Sod1 overexpression.

A. This image displays the typical traits of adult zebrafish measured to compare the macroscopic anatomy of wtSod1 and mSod1 transgenic zebrafish with Ctrl zebrafish: the standard length (SL), the length between the operculum and the caudal peduncle (LOCP) and the height at anterior of anal fin (HAA). Scale bar: 0.5 cm
B. Representative pictures of 12 months old zebrafish: an adult of the AB line with a short caudal fin (Ctrl) and zebrafish expressing either wild type Sod1 (wtSod1) or mutant Sod1 (mSod1) with long caudal fins. Adult mSod1 zebrafish present bright red eyes because of the expression of the fluorescent protein DsRed, used as reporter gene to identify mutant fish. Scale bar: 0.5 cm.
C. The histograms compare the standard length, the height at anterior of anal fin, the length between the operculum and the caudal peduncle measured in 7 Ctrl, 6 wtSod1 and 7 mSod1 fish and the body weight recorded in 15 Ctrl, 14 wtSod1 and 14 mSod1 zebrafish belonging to two different generations.

   Results were statistically analyzed with One-way Analysis of Variance (ANOVA), Kruskal-Wallis test, and corrected with Dunn's multiple comparison test. Means were considered statistically different when $P < 0.05$.

   There are no significant differences in the four parameters took under consideration among zebrafish of the three genotypes.

   Columns represent mean ± SEM of the indicated parameter.

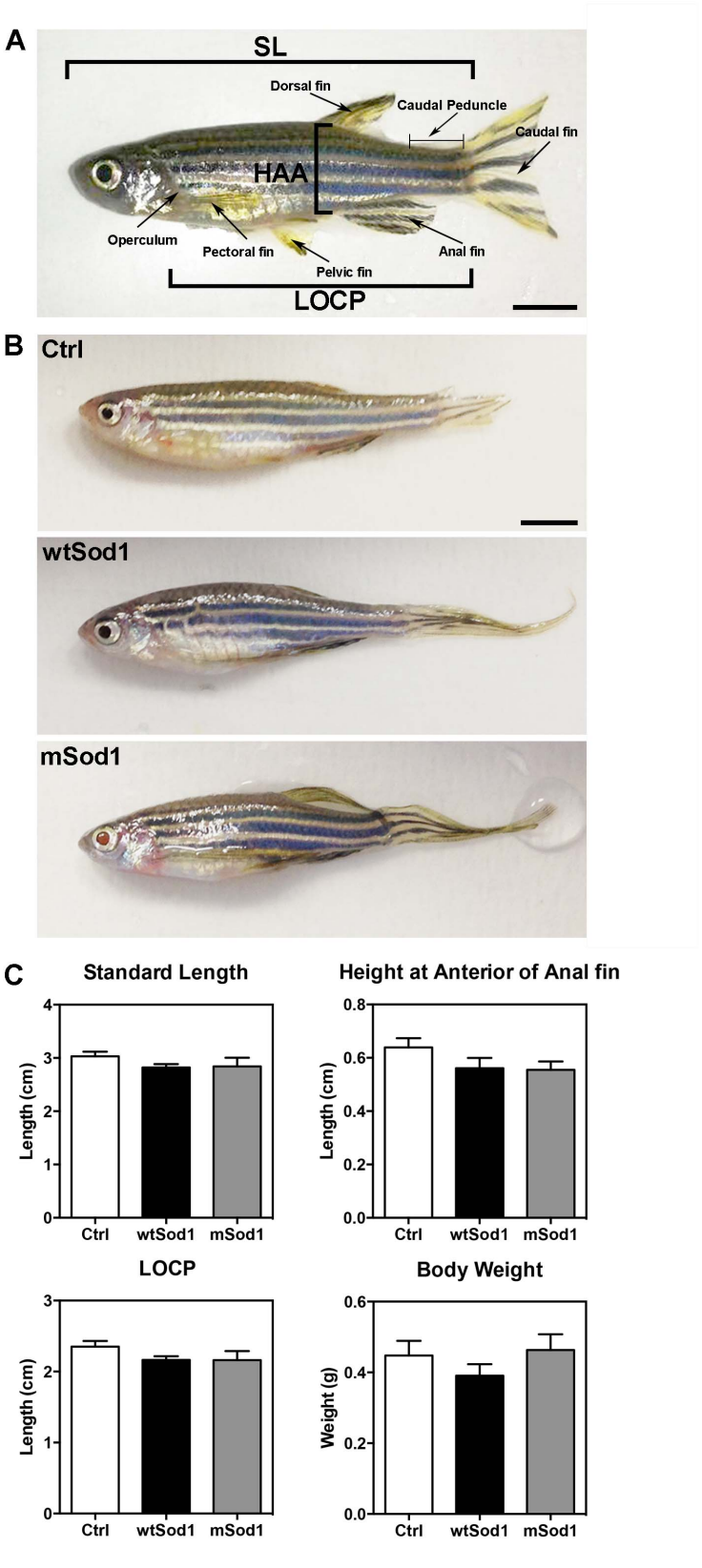
A
SL
Dorsal fin
Caudal Peduncle
Caudal fin
HAA
Operculum
Pectoral fin
Pelvic fin
Anal fin
LOCP
B
Ctrl
wtSod1
mSod1
C
Standard Length
Height at Anterior of Anal fin
Length (cm)
Ctrl
wtSod1
mSod1
LOCP
Body Weight
Weight (g)

FIGURE 2: Adult mSod1 zebrafish are compromised in their spontaneous swimming activity.

A. This image shows 3 representative paths, obtained with the MTrack2 Fiji Plugin, swum by Ctrl (in gray), wtSod1 (in blue) and mSod1 (in red) adult zebrafish in a 10 minutes period of spontaneous locomotor activity monitoring.
B. The analyses of the tracks revealed a significant reduction in the distance travelled and in the time spent at resting but not in the speed of mSod1 fish compared to Ctrl zebrafish.

   In each graph, columns represent mean ± SEM of the indicated parameter, calculated in 15 adult zebrafish for each genotype. Four independent experiments were performed with adult zebrafish belonging to two different generations.

   Measures were statistically analyzed with ordinary One-way Analysis of Variance (ANOVA) or Kruskal-Wallis test and corrected with Tukey's or Dunn's multiple comparison procedures, respectively.

   Means were considered statistically different when $P < 0.05$.

   (*, $P < 0.05$)

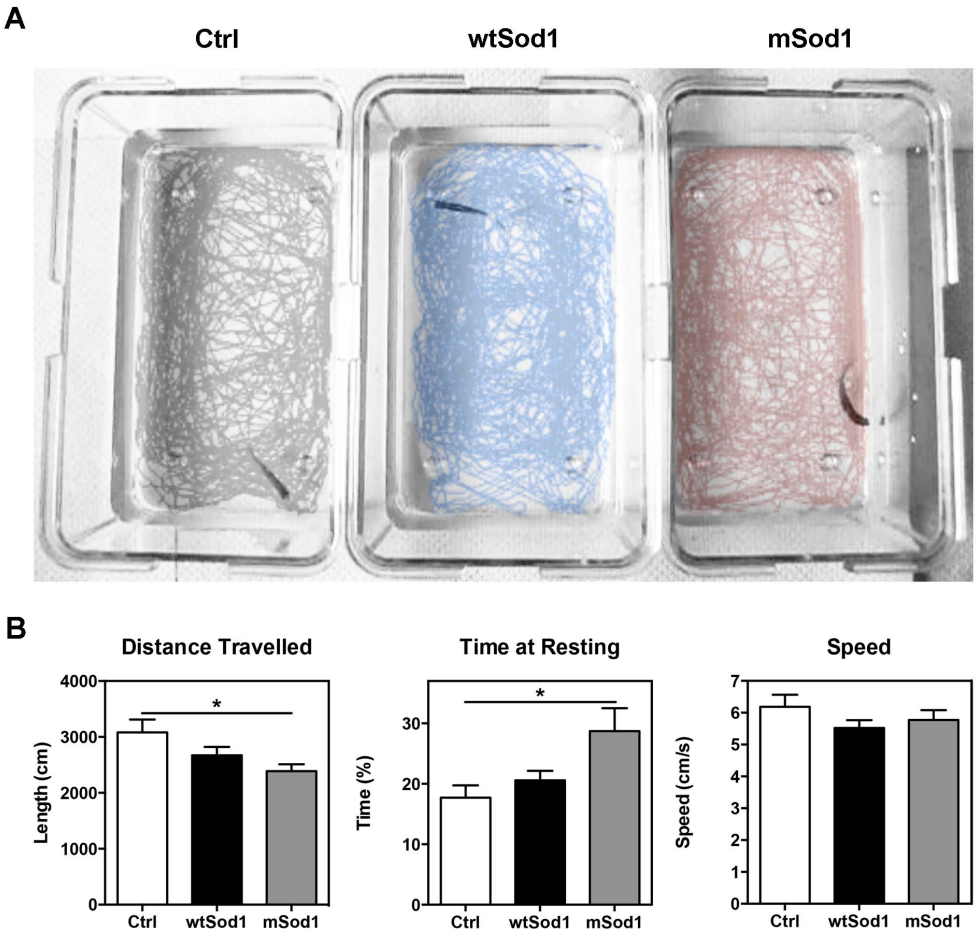
A
Ctrl
wtSod1
mSod1
B
Distance Travelled
Length (cm)
4000
3000
2000
1000
0
*
Ctrl
wtSod1
mSod1
Time at Resting
Time (%)
30
20
10
0
*
Ctrl
wtSod1
mSod1
Speed
Speed (cm/s)
7
6
5
4
3
2
1
0
Ctrl
wtSod1
mSod1

FIGURE 3: Adult mSod1 zebrafish show a significant reduction in the number of motor neurons, in the area of the spinal cord and in the caliber of white muscle fibers

A. Illustration of the zebrafish body segmentation used for the histological analyses. To precisely characterize the phenotype associated to wtSod1 and mSod1 in the spinal cord and lateral muscle of adult zebrafish trunk, we transversely cut each animal in 5 segments using fins (indicated with arrows) as standard anatomical references. Segment 1 (S1) results from a cut in correspondence of the operculum, segment 2 (S2) goes from the operculum to the beginning of the pelvic fin, segment 3 (S3) spans the pelvic fin till the beginning of the anal fin, segment 4 (S4) ranges from the beginning to the end of the anal fin and segment 5 (S5) extends from the end of the anal fin to the caudal peduncle. Scale bar: 0.5 cm.
B. Images of hematoxylin & eosin stained histological sections showing Ctrl, wtSod1 and mSod1 zebrafish spinal cord (S2 segment). In these sections we identified and counted motor neurons (one, in each sample, is indicated with an arrow head) in the ventral horns of the spinal cord. Scale bar: 50 μm.

   Plots show the significant reduction in the spinal cord area and in the motor neurons number, along the entire spinal cord, in mSod1 fish compared to both Ctrl and wtSod1 zebrafish.
C. Hematoxylin & eosin staining. Histological images showing white muscle fibers of Ctrl, wtSod1 and mSod1 zebrafish (S2 segment). They show muscular atrophy and edema (*) with infiltrating cells (arrow head) in mSod1 zebrafish lateral muscle.

   Scale bar: 25 μm.

   The plot displays a significant reduction in white muscle fibers caliber along mSod1 zebrafish trunk in comparison with Ctrl zebrafish.

Each point in the plots represents mean ± SEM of the indicated parameter calculated in each segment in at least 6 Ctrl, wtSod1 and mSod1 adult zebrafish for each genotype. Measures were statistically analyzed with Two-way Analysis of Variance (ANOVA) and corrected with Sidak's multiple comparison test.
Means were considered statistically different when $P < 0.05$.
(*, $P < 0.05$; **, $P < 0.01$; ***, $P < 0.001$).

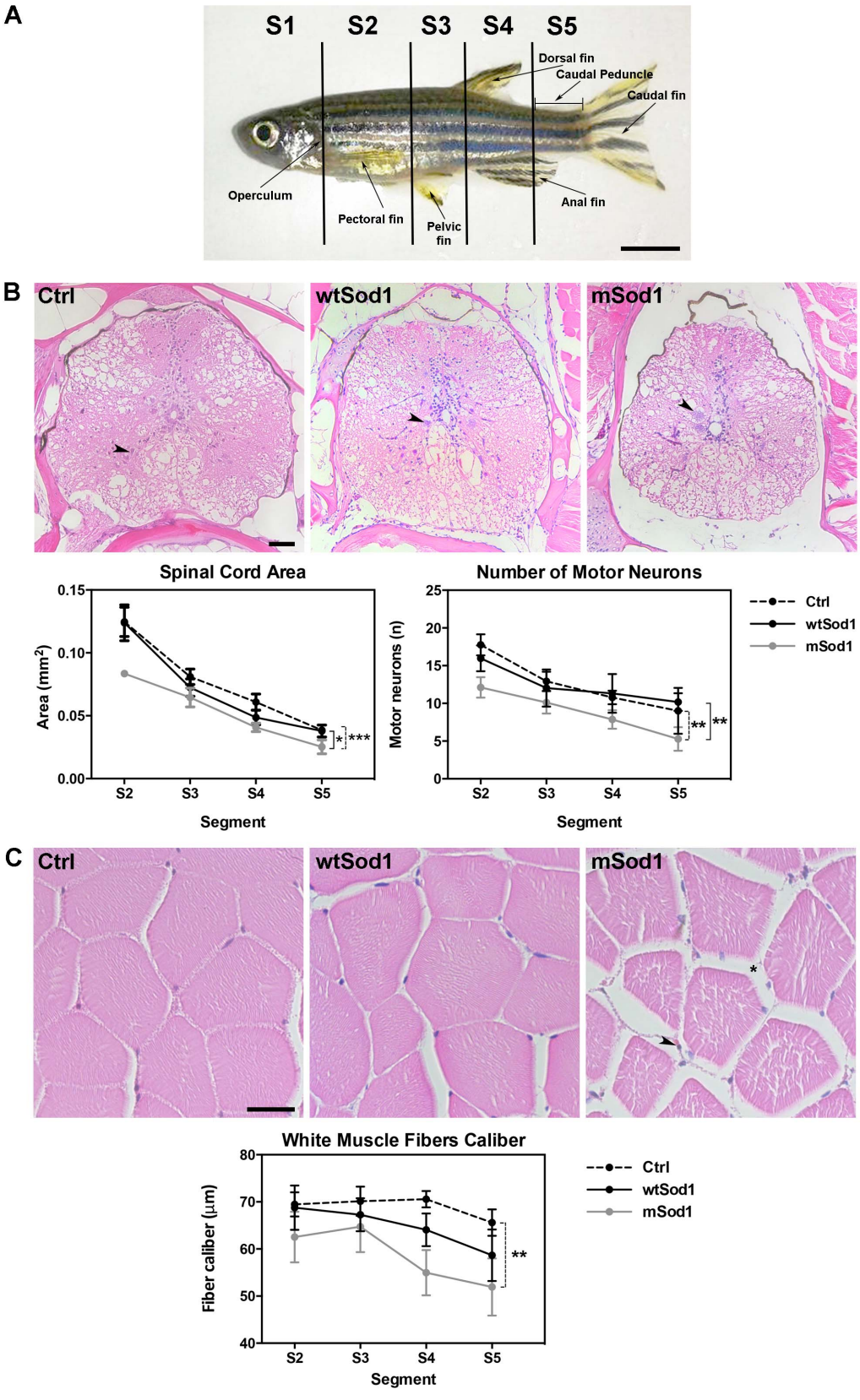
A
S1
S2
S3
S4
S5
Dorsal fin
Caudal Peduncle
Caudal fin
Operculum
Pectoral fin
Pelvic fin
Anal fin
B
Ctrl
wtSod1
mSod1
Spinal Cord Area
Area (mm²)
0.15
0.10
0.05
0.00
S2
S3
S4
S5
Segment
Number of Motor Neurons
Motor neurons (n)
25
20
15
10
5
0
Ctrl
wtSod1
mSod1
C
Ctrl
wtSod1
mSod1
White Muscle Fibers Caliber
Fiber caliber (µm)
80
70
60
50
40
Segment

FIGURE 4: Twelve months mSod1 zebrafish are compromised in lateral muscle innervation

A. These images are maximum projections of SV2A (in green) and AChRs (in red) confocal images covering the entire thickness (20 µm) of a Ctrl and of a mSod1 zebrafish lateral muscle cryosection. While in Ctrl zebrafish each postsynaptic specialization, enriched with acetylcholine receptors, faces motor nerves terminals containing several vesicle clusters; in mSod1 white lateral muscles, a lot of postsynaptic clusters lack the association with motor presynaptic terminals (white dashed boxes). Scale bar: 20 µm.
B. We measured a significant reduction in the percentage of innervation of postsynaptic specializations in mSod1 zebrafish compared to Ctrl. The 3D colocalization analysis, performed with the ImageJ plugin JACoP, on z-stacks covering the entire thickness of the lateral muscle sections, revealed a significant reduction in the presynaptic clusters density but not in postsynaptic clusters density in mSod1 fish compared to Ctrl. However, remaining pre and postsynaptic clusters of mSod1 zebrafish are not affected in their size or in the fluorescence intensity signal associated.

In each graph, columns represent mean ± SEM of the indicated parameter, calculated in 5 Ctrl and 6 mSod1 adult zebrafish for each genotype. Measures were statistically analyzed with an unpaired Student-t test.
Means were considered statistically different when $P < 0.05$.
(*, $P < 0.05$; **, $P < 0.01$)

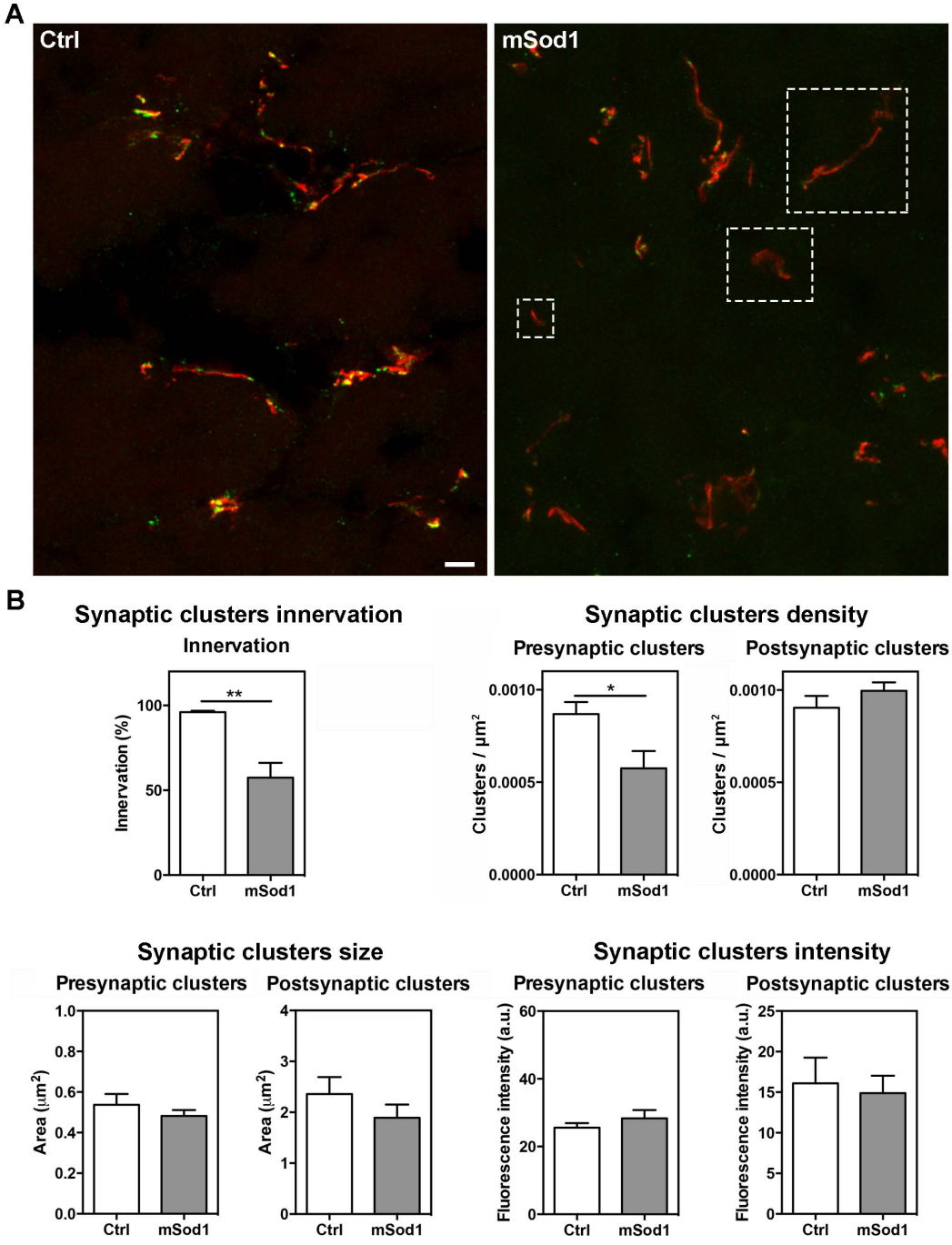
A
Ctrl
mSod1
B
Synaptic clusters innervation
Innervation
Innervation (%)
100
50
0
**
Ctrl
mSod1
Synaptic clusters density
Presynaptic clusters
Postsynaptic clusters
Clusters / µm²
0.0010
0.0005
0.0000
*
Ctrl
mSod1
Synaptic clusters size
Presynaptic clusters
Postsynaptic clusters
Area (µm²)
1.0
0.8
0.6
0.4
0.2
0.0
4
3
2
1
0
Ctrl
mSod1
Synaptic clusters intensity
Presynaptic clusters
Postsynaptic clusters
Fluorescence intensity (a.u.)
60
40
20
0
25
20
15
10
5
0
Ctrl
mSod1

FIGURE 5: Transgenic zebrafish overexpressing Sod1 show reactive astrogliosis but not microgliosis in the spinal cord and mSod1 fish present activated inflammatory cells in the white lateral muscles

A. Confocal images showing Gfap (astrocyte marker) and Aif1 (activated microglial marker) immunofluorescence staining of Ctrl, wtSod1 and mSod1 twelve months old zebrafish spinal cord histological sections (segment 4). Scale bar: 25 μm.

   We detected a significant increase in the fluorescence intensity of Gfap both in wtSod1 and mSod1 zebrafish spinal cord but no differences in Aif1 signal among zebrafish of the three genotypes. For both markers, the ratio between the mean fluorescence intensity (F.I.) and the correspondent spinal cord area in μm^2 in each segment was evaluated.

   Each point in the plots represents mean ± SEM of the indicated parameter calculated in each segment of 7 Ctrl, 6 wtSod1 and 7 mSod1 adult zebrafish for each genotype. Measures were statistically analyzed with Two-way Analysis of Variance (ANOVA) and corrected with Sidak's multiple comparison test. (*, $p < 0.05$)

B. Confocal images of a portion of Ctrl, wtSod1 and mSod1 zebrafish lateral muscle stained for Aif1 (segment 4). Scale bar: 25 μm.

   We can see how, around atrophic muscular fibers, there is an enrichment of activated macrophages and neutrophils in mSod1 zebrafish muscle compared to both wtSod1 and Ctrl zebrafish.

   The graphs show that there is a significant increase both in the number of Aif1 positive cells and in the percentage of the area covered by Aif1 positive cells in the white lateral muscle of mSod1 fish in all segments of zebrafish trunk examined.

   Each point represents mean ± SEM of the indicated parameter, calculated in 3 adult zebrafish for each genotype. Measures were statistically analyzed with Two-way Analysis of Variance (ANOVA) corrected with Sidak post-test.

   Means were considered statistically different when $P < 0.05$.

   (***, $P < 0.001$; ****, $P < 0.0001$)

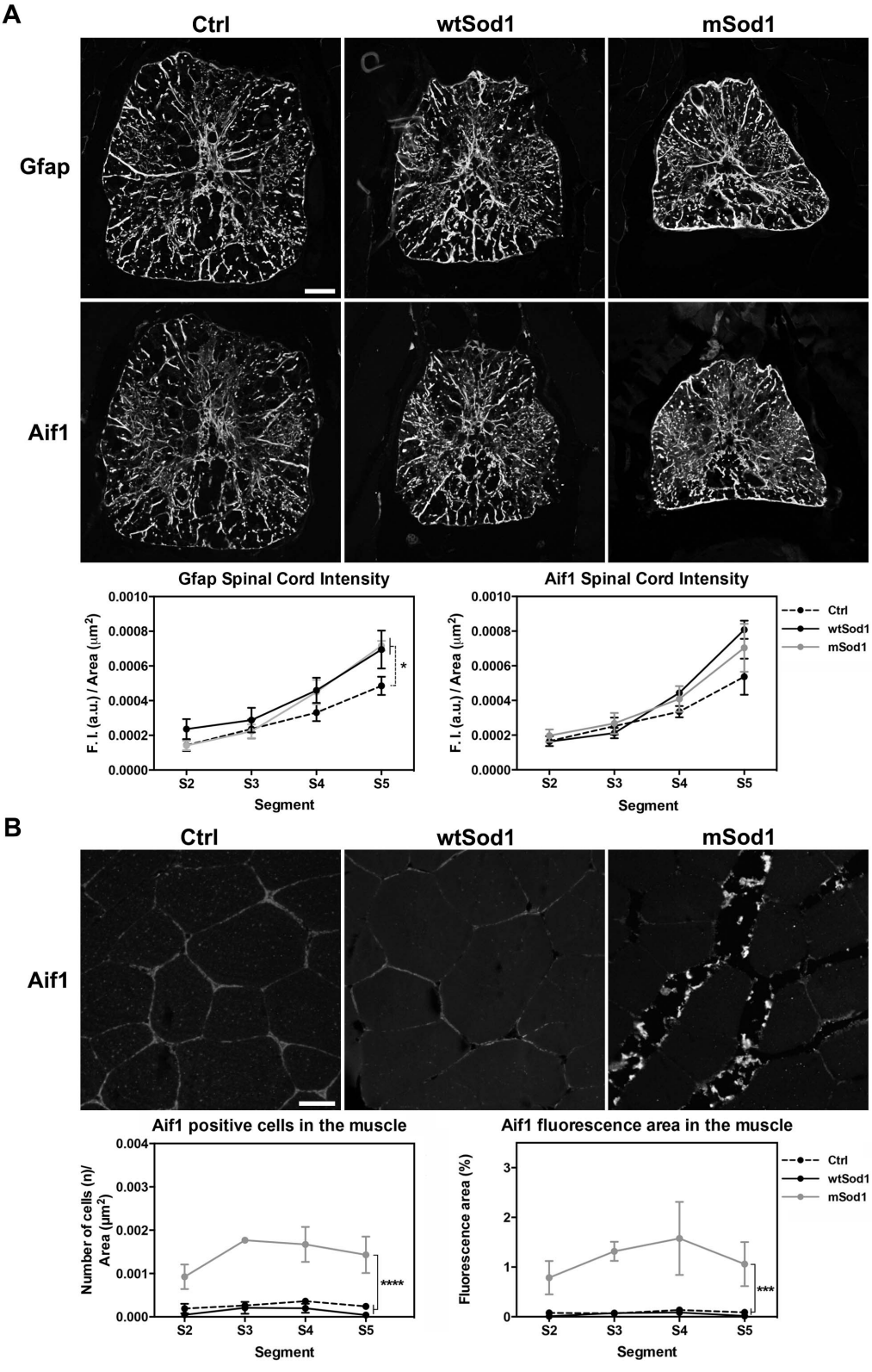
A
Ctrl
wtSod1
mSod1
Gfap
Aif1
Gfap Spinal Cord Intensity
Aif1 Spinal Cord Intensity
F. I. (a.u.) / Area (µm²)
0.0010
0.0008
0.0006
0.0004
0.0002
0.0000
S2
S3
S4
S5
Segment
*
Ctrl
wtSod1
mSod1
B
Aif1
Aif1 positive cells in the muscle
Aif1 fluorescence area in the muscle
Number of cells (n)/ Area (µm²)
0.004
0.003
0.002
0.001
0.000
****
Fluorescence area (%)
3
2
1
0
***

FIGURE 6: The expression of complex motor behaviors is associated with morphological and ultrastructural changes of the developing locomotor network

A. We morphologically characterized zebrafish locomotor network, at specific developmental stages, when embryos and larvae express peculiar motor responses. We studied embryos 20 hpf when they undergo a transient period of alternating tail coilings and 48 hpf when they respond to touch with fast coilings of the trunk and larvae 96 hpf when they start swimming.
B. Ctrl embryos 24 hpf show short motor axons, protruding from the spinal cord, filled with synaptic vesicles (green) travelling along the entire axonal length. Motor axons outgrowth follows a rostral to caudal developmental wave and only more rostral motor nerves present branches. Acetylated tubulin (gray) stains few spinal interneurons axonal projections. At this developmental stage, we do not detect AChRs clusters along muscular fibers precursors plasmamembrane. Scale bar: 20 μm.
C. The ultrastructural analysis shows axonal projections filled with synaptic vesicles (sv), with immature boutons (B) facing muscular fibers precursors presenting a cytoplasm filled with glycogen (square box) and where the contractile apparatus is poorly organized. Scale bar: 500 nm.
D. At 48 hpf, motor nerves present a well organized microtubule network along their entire length. They deeply protrude in the trunk along miosepta and start innervating muscular fiber precursors with several branches. Synaptic vesicles do not follow the entire axonal length but are well organized in small clusters at the tips of axonal branches. AChRs (red) start organizing in visible clusters on muscular fibers.
E. Electron micrographs show presynaptic terminals, filled with vesicles (sv), mainly located at the periphery of myotomes. Muscle fiber precursors now display a well-organized contractile apparatus (S).
F. Larvae 96 hpf show well developed motor nerves, heavily branched, innervating muscle fibers. Synaptic vesicles are distributed in small clusters at the tips of axonal terminals and now face AChRs clusters on muscle fibers (their superimposition generate a yellow signal in the merged image).
G. The ultrastructural analysis shows small presynaptic boutons (B) deeply penetrating inside the myotome and innervating well-developed muscle fibers.

Confocal images are maximum projection of z-stacks covering half zebrafish trunk.

Symbols: B: presynaptic bouton; AZ: Active Zone; sv: synaptic vesicle; M presynaptic mitochondria; m: muscular mitochondria; e: endosome; S: sarcomere.

A

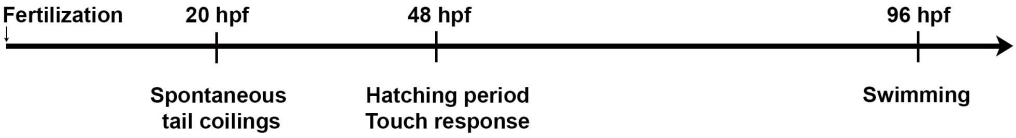

B Embryo 24 hpf

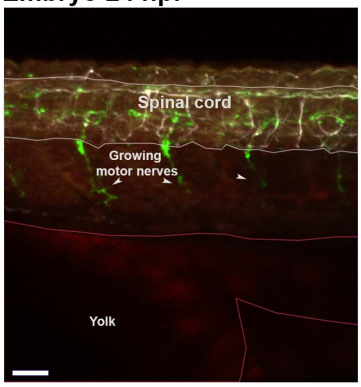

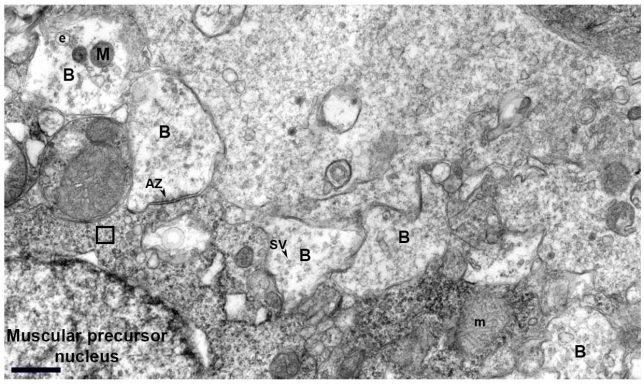

C Embryo 48 hpf

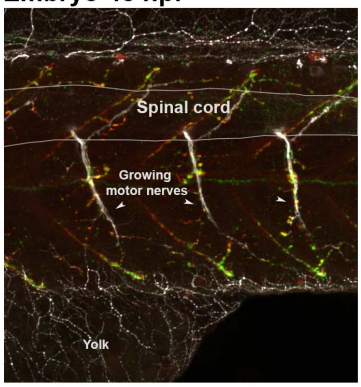

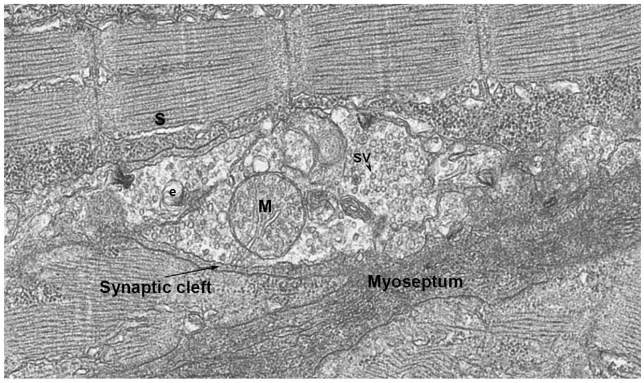

D Larvae 96 hpf

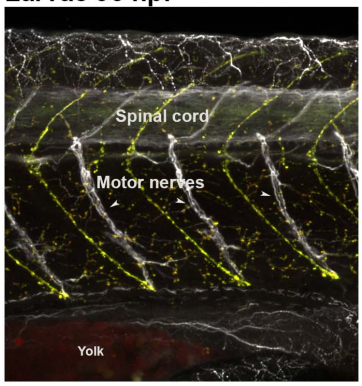

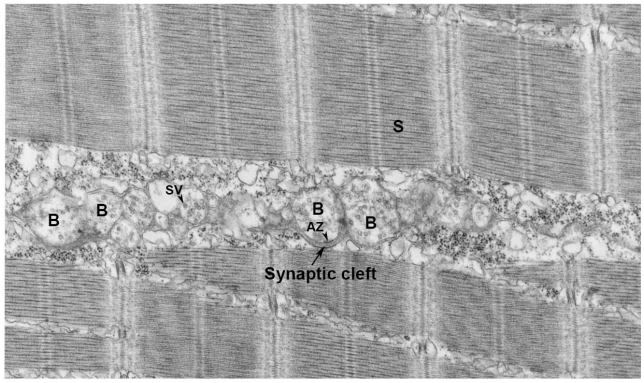

FIGURE 7: The overexpression of Sod1 causes precocious motor axons alterations

A. Confocal fluorescence maximum projection images showing SV2A signal (in green). They cover the entire Ctrl, wtSod1 and mSod1 zebrafish trunk of 24 hpf embryos in a region ranging from the 12^{th} and the 16^{th} somite.
   Since synaptic vesicles travel along the entire axonal length (traced with a dashed line), we can appreciate motor axons length and motor nerves branches in embryos of the three genotypes.
   Scale bar: 25 μm.
B. We measured a significant reduction in the motor axons length and in the unbranched axonal length in both wtSod1 and mSod1 embryos compared to Ctrl fish but a significant increase in the number of motor nerves branches only in mSod1 embryos compared to both Ctrl and wtSod1 zebrafish.
   Columns represent mean ± SEM of the indicated parameter, calculated in 25 Ctrl, 17 wtSod1 and 21 mSod1 embryos for each genotype. Measures were statistically analyzed with One-way Analysis of Variance (ANOVA) or Kruskal-Wallis test and corrected with Tuckey's or Dunn's multiple comparison test, respectively.
   Means were considered statistically different when $P < 0.05$.
   (*, $P < 0.05$; ***, $P < 0.001$; ****, $P < 0.0001$)

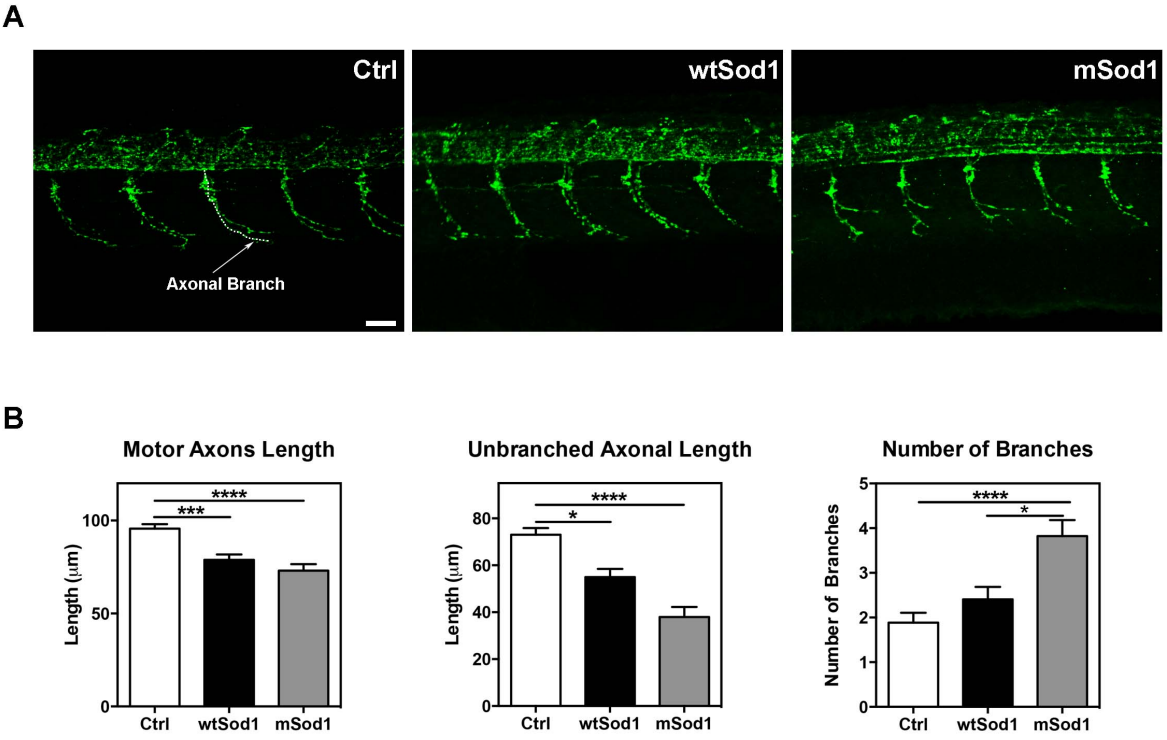
A
Ctrl
wtSod1
mSod1
Axonal Branch
B
Motor Axons Length
Length (µm)
****
***
100
50
0
Ctrl
wtSod1
mSod1
Unbranched Axonal Length
Length (µm)
****
*
80
60
40
20
0
Ctrl
wtSod1
mSod1
Number of Branches
Number of Branches
****
*
5
4
3
2
1
0
Ctrl
wtSod1
mSod1

FIGURE 8: Sod1 overexpressing embryos do not show alterations in motor nerves morphology 48 hpf but those expressing G93R Sod1 present defects in synaptic vesicles clusterization

A. This panel illustrates the morphological features of Ctrl and mSod1 motor nerves 48 hpf. At this developmental stage, acetylated tubulin (gray) outlines spinal motor axons and allows the measurement of motor axons length and branches. Synaptic vesicles (green) do not depict the entire axonal length but are organized in big clusters along the main axonal path or are arranged in small clusters at the tips of axonal branches. AChRs (red) are organized in big clusters in muscular precursors plasmamembrane, both in correspondence of the myoseptum where motor axons go through, but also deeply inside the myotome. These are confocal fluorescence maximum projection images of acetylated tubulin (gray), SV2A (green), AChRs (red) and their merge covering half zebrafish trunk in correspondence of the 9^{th} and the 13^{th} somite.
   Scale bar: 25 μm.
B. The analyses of motor nerves morphology did not reveal any alteration in motor axons length, unbranched axonal length (not shown) and number of branches among embryos of the 3 genotypes. Columns represent mean ± SEM of the indicated parameter, calculated in 10 Ctrl, 10 wtSod1 and 13 mSod1 embryos for each genotype. Measures were statistically analyzed with One-way Analysis of Variance (ANOVA) and corrected with Tuckey's multiple comparison post-test. Means were considered statistically different when $P < 0.05$.
C. D. E. The 3D object based colocalization analyses did not reveal any differences either in the density of total presynaptic and colocalizing presynaptic clusters (C) or in the density of total postsynaptic and postsynaptic colocalizing clusters (E) but showed a significant increase in presynaptic clusters area in mSod1 compared to Ctrl and wtSod1 embryos (D). Postsynaptic clusters dimension does not change (D).
   Columns represent mean ± SEM of the indicated parameter, calculated in 10 Ctrl, 9 wtSod1 and 13 mSod1 embryos for each genotype. Measures were statistically analyzed with Kruskal-Wallis test and corrected with Dunn's multiple comparison procedure. Means were considered statistically different when $P < 0.05$.
   (*, $P < 0.05$)

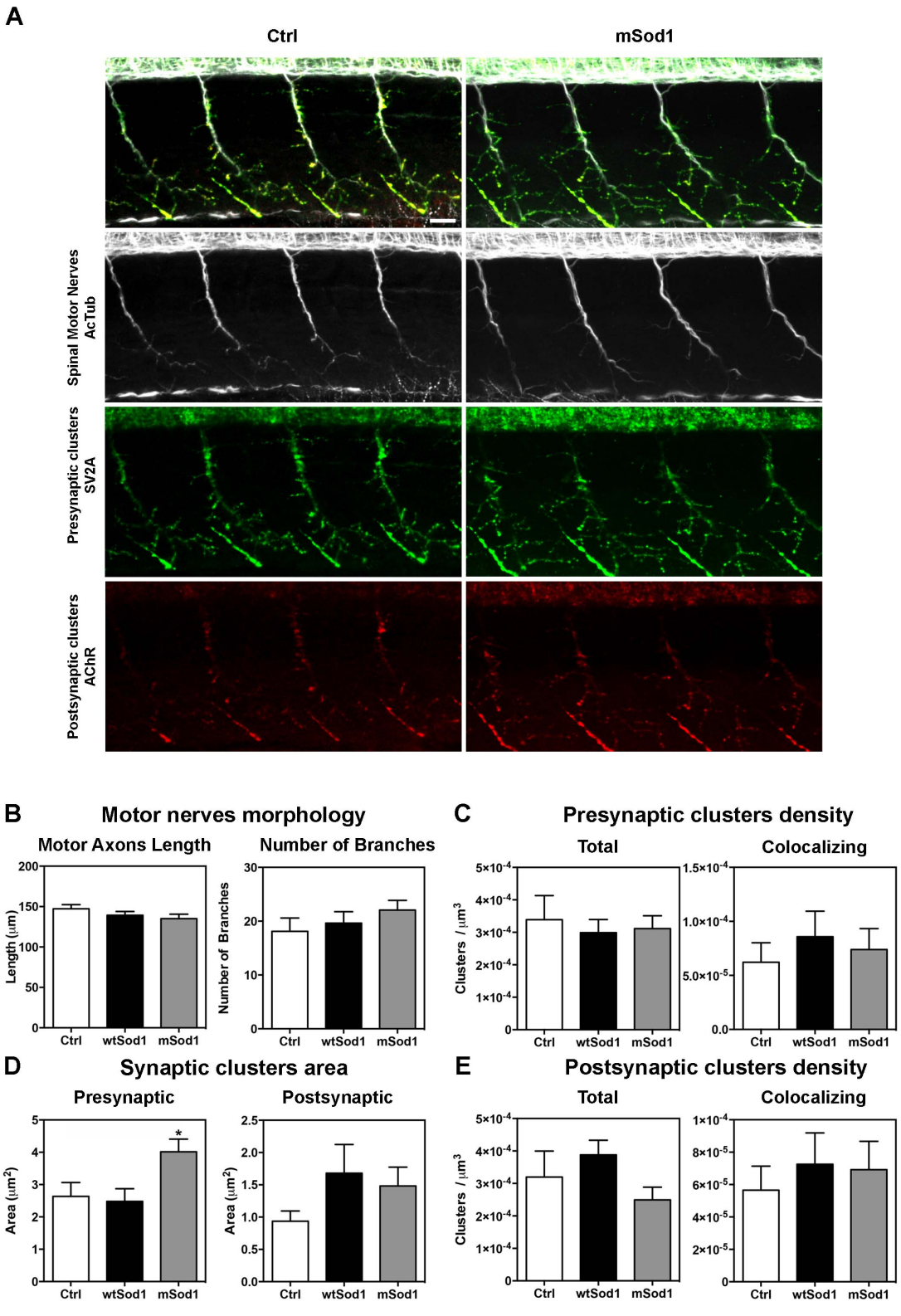
A
Ctrl
mSod1
Spinal Motor Nerves AcTub
Presynaptic clusters SV2A
Postsynaptic clusters AChR
B
Motor nerves morphology
Motor Axons Length
Number of Branches
Length (µm)
Number of Branches
Ctrl
wtSod1
mSod1
C
Presynaptic clusters density
Total
Colocalizing
Clusters / µm3
D
Synaptic clusters area
Presynaptic
Postsynaptic
Area (µm2)
E
Postsynaptic clusters density
Total
Colocalizing
Clusters / µm3

FIGURE 9: mSod1 larvae exhibit a severe impairment in neuromuscular junctions maturation 96 hpf

A. These images display the phenotype of Ctrl, wtSod1 and mSod1 neuromuscular junctions at 96 hpf. They are confocal fluorescence maximum projection images of SV2A (green), AChRs (red) and their merge covering half zebrafish trunk in correspondence of the 10th and the 15th somite. Scale bar: 25 μm.
B. The analyses of pre and postsynaptic clusters dimensions revealed no more differences in the mean area of both type of synaptic clusters at this stage of development. However, the 3D object based colocalization analysis showed a significant reduction in the density of presynaptic SV2A clusters in mSod1 larvae musculature compared to both Ctrl and wtSod1 larvae but not in the density of postsynaptic clusters. Moreover, it evidenced a significant reduction both in presynaptic and postsynaptic colocalizing clusters in mSod1 larvae compared to both wtSod1 and Ctrl fish highlighting impairments in neuromuscular junctions formation.
Columns represent mean ± SEM of the indicated parameter, calculated in 19 Ctrl, 12 wtSod1 and 16 mSod1 embryos for each genotype. Measures were statistically analyzed with Kruskal-Wallis test and corrected with Dunn's multiple comparison procedure. Means were considered statistically different when $P < 0.05$.
(*, $P < 0.05$; ***, $P < 0.001$)

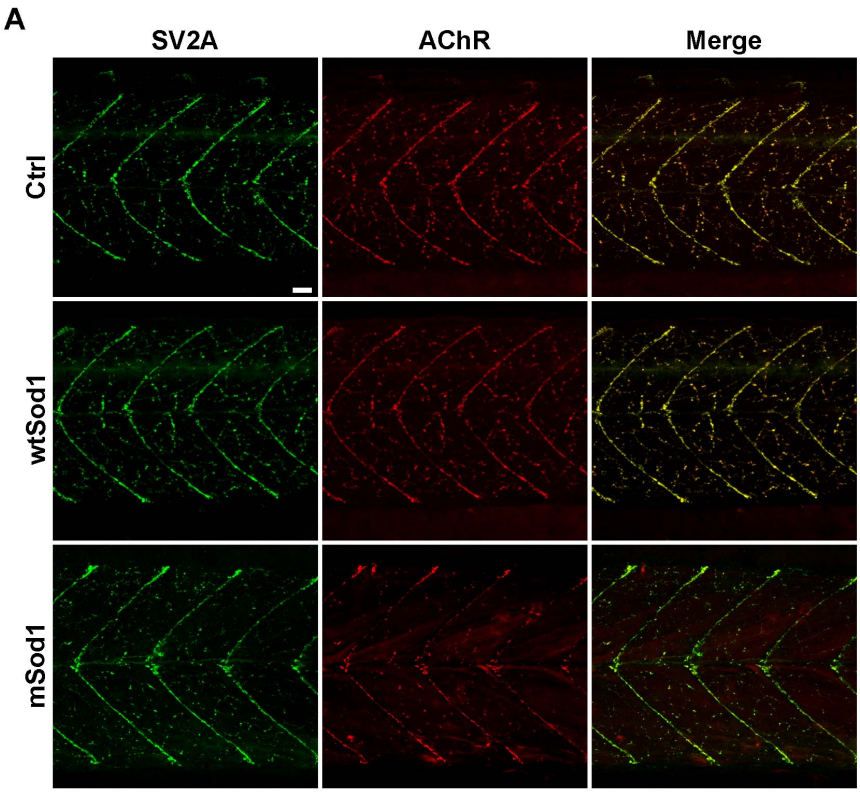
A
SV2A
AChR
Merge
Ctrl
wtSod1
mSod1

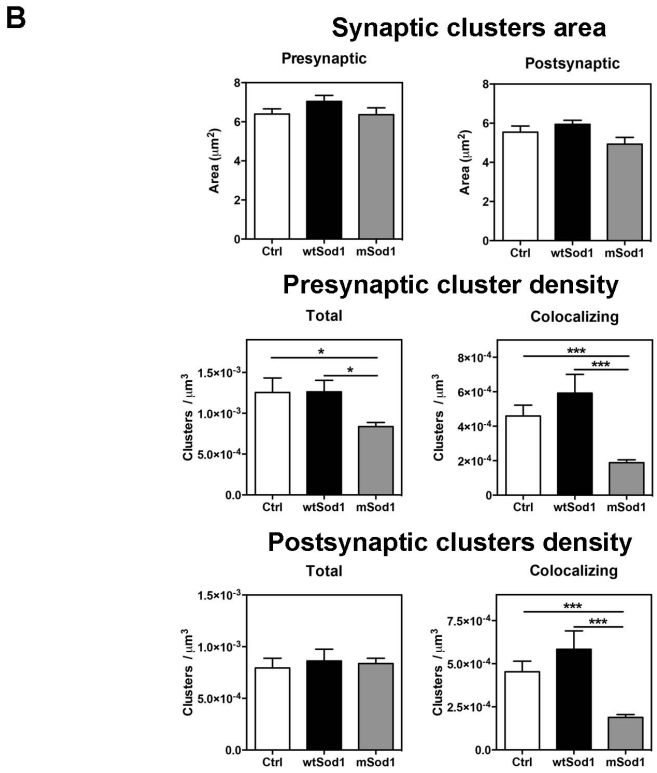
B
Synaptic clusters area
Presynaptic
Postsynaptic
Area (µm²)
Ctrl
wtSod1
mSod1
Presynaptic cluster density
Total
Colocalizing
Clusters / µm³
Postsynaptic clusters density
Total
Colocalizing
Clusters / µm³

FIGURE 10: The ultrastructure of mSod1 neuromuscular junctions is preserved 96 hpf

A. Electron micrographs showing the ultrastructure of Ctrl, wtSod1 and mSod1 neuromuscular junctions of 96 hpf zebrafish larvae. Presynaptic boutons contain a lot of vesicles (indicated with a chevron >) widely distributed in the presynaptic terminal without a peculiar polarization. Some of them are fusing in correspondence of the active zones (AZ). Presynaptic terminals include mitochondria (m) and are separated from the muscle fibers by a well-defined synaptic cleft (sc). Zebrafish neuromuscular junctions do not present evident postsynaptic specializations. In muscle fibers we can observe well-organized sarcomeres (s). Scale bar: 200 nm.
B. Morphometric analyses did not reveal any differences in the area of neuromuscular junctions, in the density and morphology of synaptic vesicles (diameter and circularity, area and perimeter –not shown-) and in the number and morphology of mitochondria (diameter and circularity, area and perimeter –not shown-) in the presynaptic terminals among larvae of the three genotypes.

   Histograms columns represent mean ± SEM of the indicated parameter. The features measured in the morphometric analyses were evaluated in 30 neuromuscular junctions belonging to 3 different animals for each genotype. Measures were statistically analyzed with Kruskal-Wallis test and corrected with Dunn's multiple comparison procedure.

   Means were considered statistically different when $P < 0.05$.

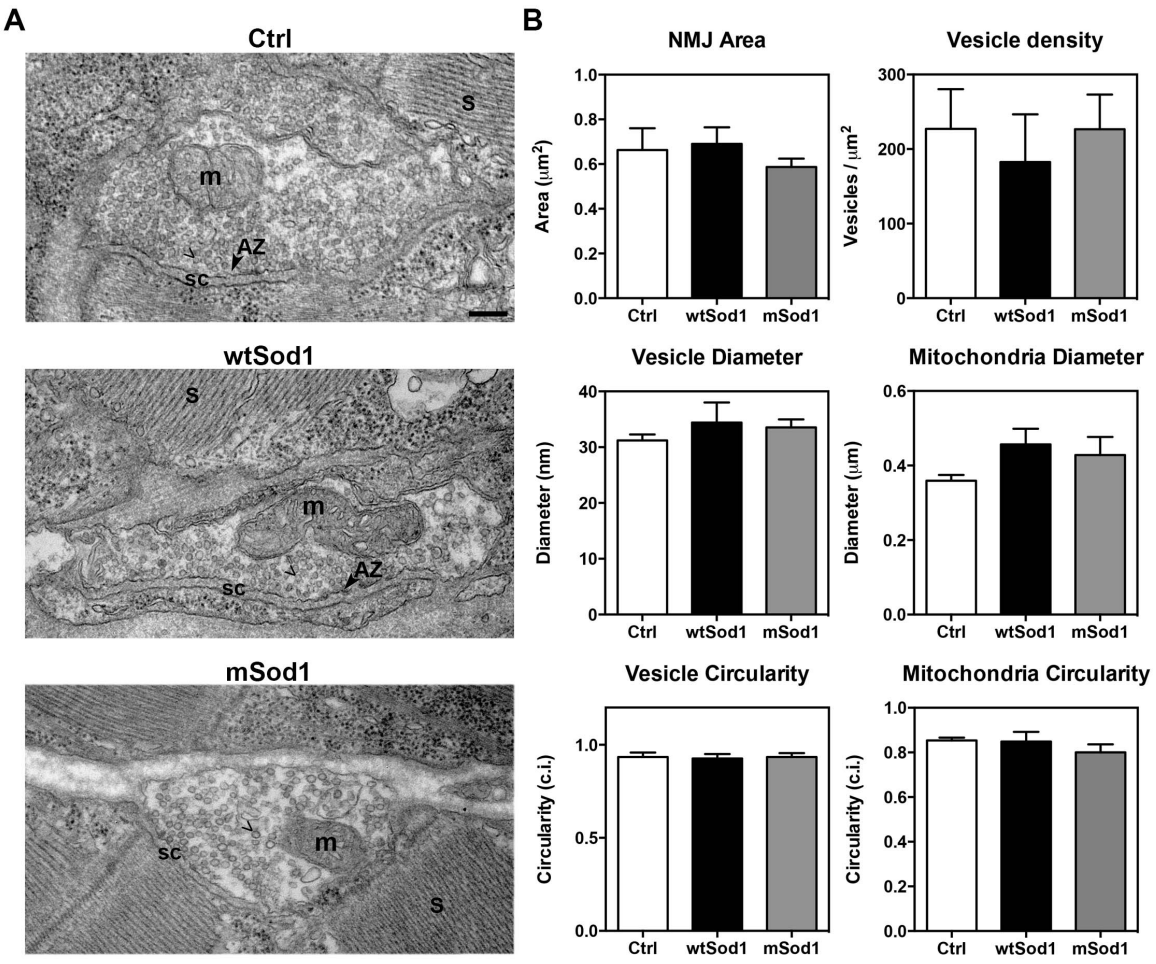
A
Ctrl
s
m
AZ
sc
wtSod1
s
m
AZ
sc
mSod1
sc
m
s
B
NMJ Area
Area (μm²)
1.0
0.8
0.6
0.4
0.2
0.0
Ctrl
wtSod1
mSod1
Vesicle density
Vesicles / μm²
300
200
100
0
Ctrl
wtSod1
mSod1
Vesicle Diameter
Diameter (nm)
40
30
20
10
0
Ctrl
wtSod1
mSod1
Mitochondria Diameter
Diameter (μm)
0.6
0.4
0.2
0.0
Ctrl
wtSod1
mSod1
Vesicle Circularity
Circularity (c.i.)
1.0
0.5
0.0
Ctrl
wtSod1
mSod1
Mitochondria Circularity
Circularity (c.i.)
1.0
0.8
0.6
0.4
0.2
0.0
Ctrl
wtSod1
mSod1

FIGURE 11: Larvae expressing mSod1 present a significant reduction in muscle fibers caliber and mitochondrial area with a preservation of the sarcomere ultrastructure

A. Maximum projection of the myosin Second Harmonic Generation (SHG) signal images collected from half mSod1 larva trunk in correspondence of the 12^{th} and the 15^{th} somite. Scale bar: 25 μm.
B. Myosin SHG signal images of Ctrl, wtSod1 and mSod1 muscle fibers, acquired in corresponding depths of the myotome, showing the endogenous myosin signal used for the quantification of muscle fibers caliber. Scale bar: 20 μm. We measured a significant reduction in muscle fibers caliber in mSod1 larvae compared to Ctrl. Columns represent mean ± SEM of the indicated parameter, calculated in 17 Ctrl, 15 wtSod1 and 18 mSod1 larvae for each genotype. Statistical analysis was performed with One-way Analysis of Variance (ANOVA) and Tuckey's multiple comparison test. Means were considered statistically different when $P < 0.05$.
   (**, $P < 0.01$)
C. This panel displays a detail of myosin SHG signal showing the organization of sarcomeres in Ctrl, wtSod1 and mSod1 muscle fibers. Scale bar: 5 μm. The measure of the distance between two minima (red line in graphs) in the myosin SHG signal intensity plot profiles obtained along the longitudinal axis of the fibers allowed us to assess that the length of sarcomeres do not change.
D. Electron micrographs showing the preserved sarcomere ultrastructure in Ctrl, wtSod1 and mSod1 larvae at 96 hpf. Scale bar: 1 μm.
   The measure of 100 sarcomeres, in 2 animals per genotype, confirmed the preserved sarcomere length. Measures were statistically analyzed with One-way Analysis of Variance (ANOVA) and corrected with Tuckey's post-test. Means were considered statistically different when $P < 0.05$.
E. These electron micrographs display muscular mitochondria (m) morphology in Ctrl, wtSod1 and mSod1 larvae. Scale bar: 1 μm. We measured a significant reduction in the area of muscular mitochondria but not in the perimeter and circularity in mSod1 larvae. We analyzed 100 mitochondria in 6 Ctrl, 4 wtSod1 and 6 mSod1 larvae. Measures were statistically analyzed with One-way Analysis of Variance (ANOVA) and corrected with Tuckey's multiple comparison tests. Means were considered statistically different when $P < 0.05$. (*, $P < 0.05$)

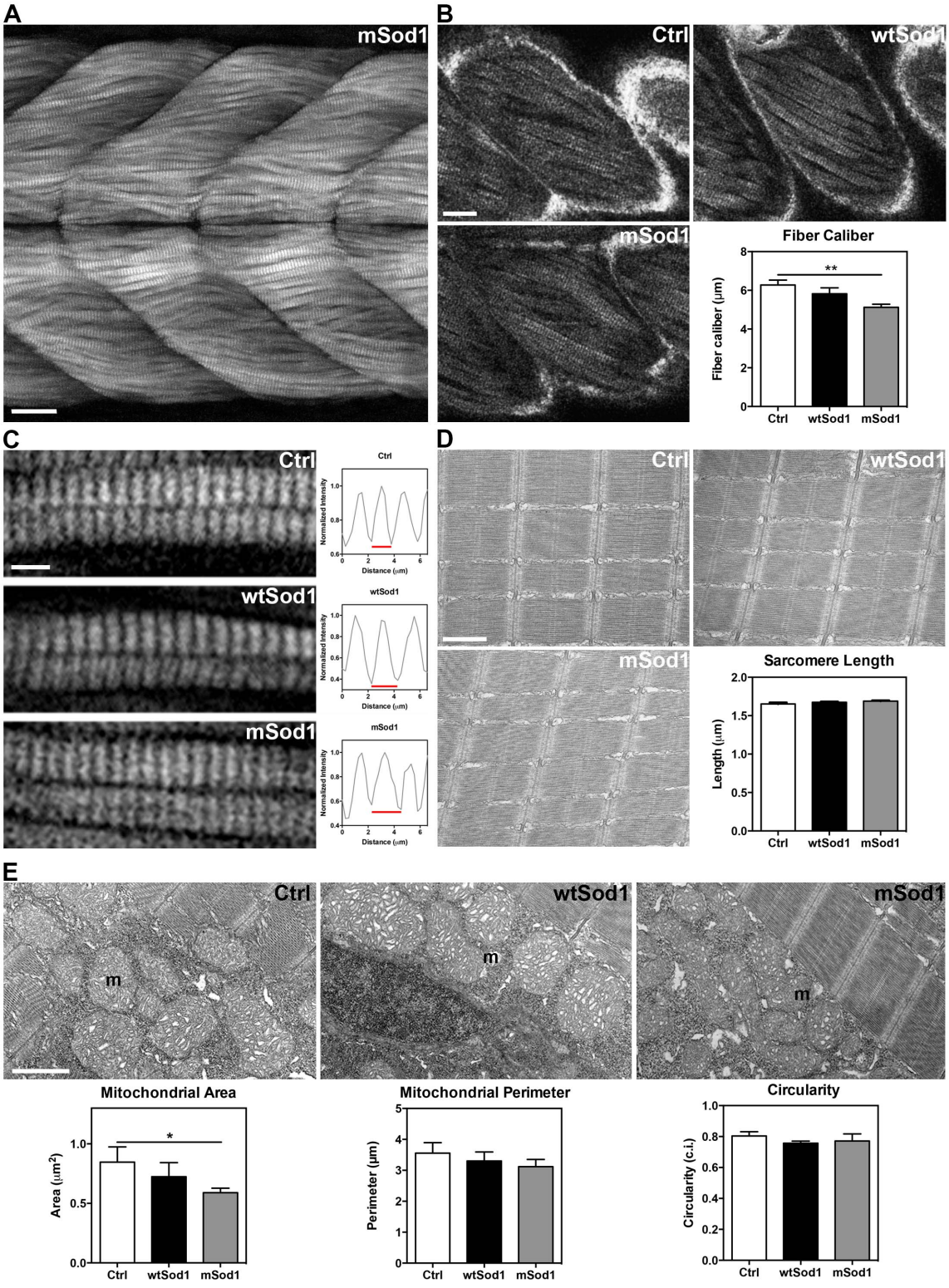
A
mSod1
B
Ctrl
wtSod1
mSod1
Fiber Caliber
Fiber caliber (μm)
**
Ctrl
wtSod1
mSod1
C
Ctrl
wtSod1
mSod1
Normalized Intensity
Distance (μm)
D
Ctrl
wtSod1
mSod1
Sarcomere Length
Length (μm)
E
Ctrl
wtSod1
mSod1
m
Mitochondrial Area
Area (μm²)
*
Mitochondrial Perimeter
Perimeter (μm)
Circularity
Circularity (c.i.)

FIGURE 12: mSod1 embryos display an increased frequency of spontaneous tail coilings at 20 hpf

A. Spontaneous tail coilings behavior was analyzed at 20 hpf positioning dechorionated embryos in niches engraved in a 3.5 mm round petri dish.
B. We observed a significant increase in the frequency of spontaneous tail coilings in mSod1 embryos compared to Ctrl embryos.
C. The 89.8% of mSod1 embryos performed multiple tail coilings (two consecutive repeated bends of the trunk before returning to the resting condition) compared to the 64.6% of Ctrl and the 66.6% of wtSod1 embryos. Moreover, the percentage of multiple tail coilings in mSod1 embryos is significantly higher compared to both Ctrl and wtSod1 embryos.
D. The 43.5% of mSod1 embryos performed complex coilings (several consecutive repeated bends of the trunk before returning to the resting condition) compared to the 6.3% of Ctrl and the 2.8% of wtSod1 embryos. Even the percentage of complex coilings in mSod1 embryos is significantly higher compared to both Ctrl and wtSod1 embryos.
E. While Ctrl and wtSod1 embryos performed the same percentage of alternating left-right bends of the entire body and tail bends on the same side of the body, mSod1 embryos exhibited a significant higher percentage of tail coilings on the same side of the body.

Columns represent mean ± SEM of the indicated parameter, calculated in 47 Ctrl, 36 wtSod1 and 46 mSod1 embryos for each genotype. Measures were statistically analyzed with One-way Analysis of Variance (ANOVA) or Kruskal-Wallis test and corrected with Tuckey's or Dunn's multiple comparison test. The comparison of the relative percentage of alternate versus same side tail bends was performed with Student-t test. Means were considered statistically different when $P < 0.05$.
(**, $P < 0.01$; ***, $P < 0.001$)

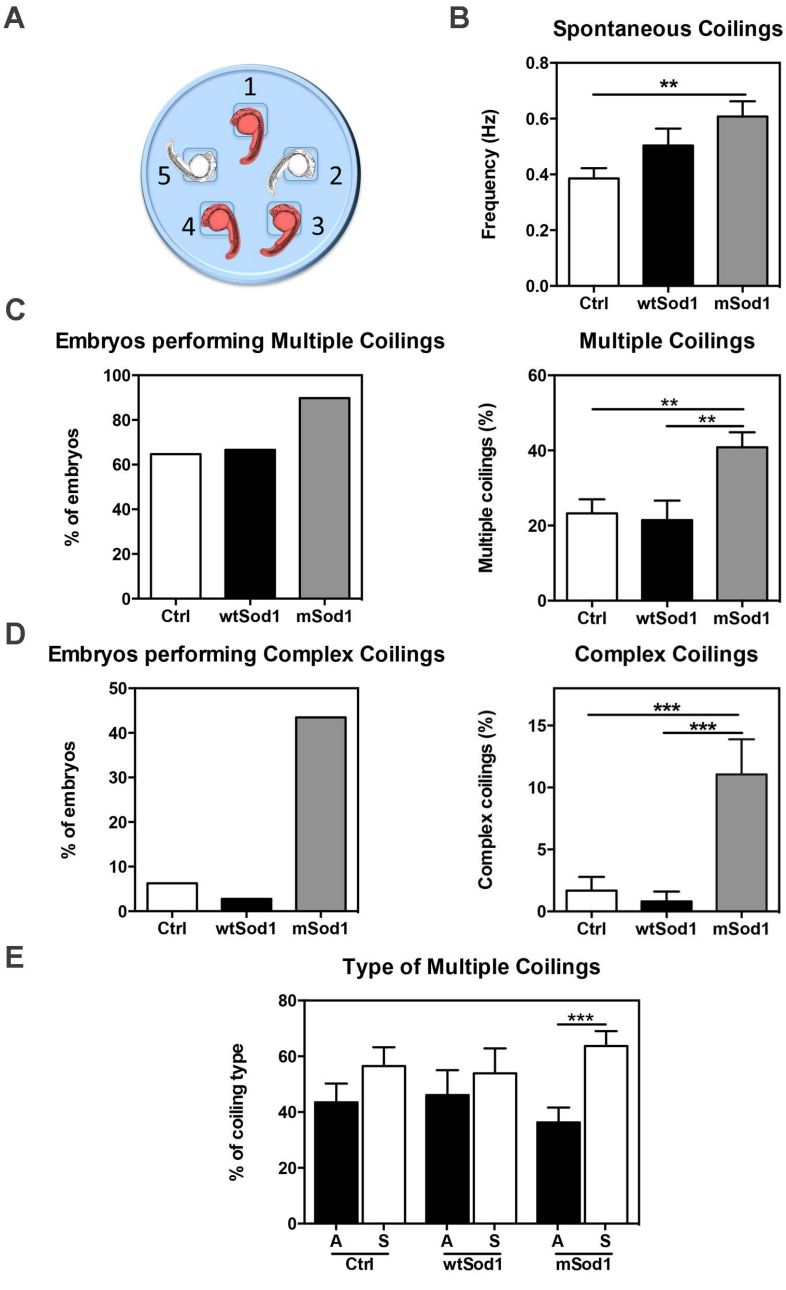
A
B
Spontaneous Coilings
Frequency (Hz)
0.8
0.6
0.4
0.2
0.0
**
Ctrl
wtSod1
mSod1
1
2
3
4
5
C
Embryos performing Multiple Coilings
% of embryos
100
80
60
40
20
0
Ctrl
wtSod1
mSod1
Multiple Coilings
Multiple coilings (%)
60
40
20
0
**
**
Ctrl
wtSod1
mSod1
D
Embryos performing Complex Coilings
% of embryos
50
40
30
20
10
0
Ctrl
wtSod1
mSod1
Complex Coilings
Complex coilings (%)
15
10
5
0
***
***
Ctrl
wtSod1
mSod1
E
Type of Multiple Coilings
% of coiling type
80
60
40
20
0
***
A
S
A
S
A
S
Ctrl
wtSod1
mSod1

FIGURE 13: mSod1 embryos present aberrant touch evoked tail coilings responses at 48 hpf

A. Ctrl, wtSod1 or mSod1 embryos at 48 hpf were embedded in a small drop of low melting-point-agarose and oriented with the dorsal side up and with the belly facing the bottom of the petri dish. When the agarose solidified, we gently removed all the agarose behind the yolk ball and we added a drop of water on the top of the fish. At least 5 tail coilings were evoked touching the trunk of the embryo above the yolk ball with the tip of a microloader and the duration of the responses and the maximum angle of tail flexion were analyzed. Scale bar: 500 μm.
B. mSod1 embryos exhibited a significant increase in the duration of touch evoked tail coilings responses and a significant decrease in the maximum angle of tail flexion compared to Ctrl and wtSod1 embryos.

   Columns represent mean ± SEM of the indicated parameter, calculated in 19 Ctrl, 14 wtSod1 and 16 mSod1 embryos for each genotype. Measures were statistically analyzed with One-way Analysis of Variance (ANOVA) and corrected with Tuckey's multiple comparison test or Kruskal-Wallis test and corrected with Dunn's post-test. Means were considered statistically different when $P < 0.05$.

   (**, $P < 0.01$; ***, $P < 0.001$; ****, $P < 0.0001$)
C. These images show representative examples of the tail flexion recorded in a single touch evoked response in Ctrl, wtSod1 and mSod1 embryos.

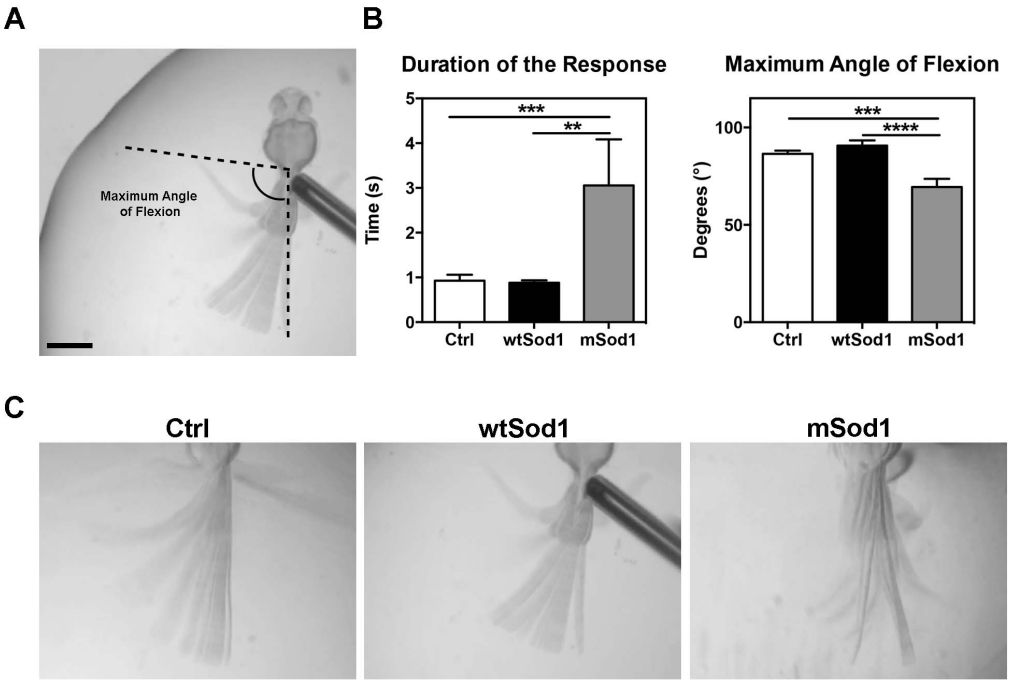
A
B
Maximum Angle
of Flexion
Duration of the Response
Time (s)
0
1
2
3
4
5
***
**
Ctrl
wtSod1
mSod1
Maximum Angle of Flexion
Degrees (°)
0
50
100
***
****
Ctrl
wtSod1
mSod1
C
Ctrl
wtSod1
mSod1

FIGURE 14: mSod1 larvae exhibit altered touch evoked swimming activity at 96 hpf

A. Schematic representation of the experimental setup used to test touch evoked swimming responses. Larvae at 96 hpf were individually transferred in a 10 mm petri dish placed on a mesh of 0.5 x 0.5 cm squares. Touch evoked swimming responses were elicited touching the trunk of the larvae with the tip of a microloader and recorded with high-resolution movies obtained with a digital camera. A representative response for Ctrl, wtSod1 and mSod1 larvae is drawn in red.
B. We measured a significant increase in the duration of the evoked swimming responses and in the distance travelled by mSod1 larvae compared to Ctrl and wtSod1 fish. Since these responses, in mSod1 larvae, consist in repeated consecutive burst swimming events, the overall speed of mSod1 responses results significantly lower compared to Ctrl and wtSod1 fish.

   Histograms columns represent mean ± SEM of the indicated parameter, calculated in 19 Ctrl, 19 wtSod1 and 19 mSod1 larvae for each genotype. Measures were statistically analyzed with One-way Analysis of Variance (ANOVA) or Kruskal-Wallis test and corrected with Tuckey's or Dunn's post test. Means were considered statistically different when $P < 0.05$.

   (*, $P < 0.05$; ***, $P < 0.001$; ****, $P < 0.0001$)

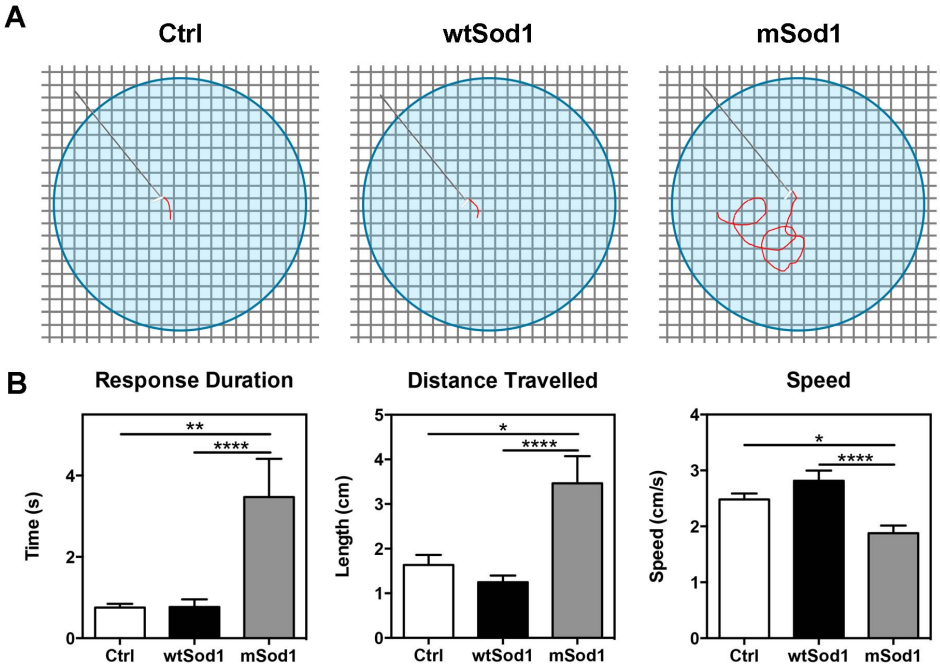
A
Ctrl
wtSod1
mSod1
B
Response Duration
Distance Travelled
Speed
Time (s)
Length (cm)
Speed (cm/s)
**
****
*
****
*
****
Ctrl
wtSod1
mSod1

FIGURE 15: Riluzole treatment reverts motor phenotype at 20 hpf and normalizes motor axons length at 24 hpf in mSod1 embryos

A. Flow chart showing the protocol followed to correlate embryos behavior at 20 hpf and spinal nerves morphology at 24 hpf. A mixed population of transgenic and non-transgenic embryos, generated intercrossing heterozygous mSod1 zebrafish (A), where placed in the niches engraved in a petri dish and spontaneous tail coilings were recorded in fish water and after the addition of riluzole or vehicle solution without displacing the embryos from their position (B). At the end of the experiment, each fish was individually transferred in a tube, fixed and stained for immunofluorescence and then visualized at the confocal microscope (C). When the images acquisition was completed, each fish was singularly collected in a tube, its DNA was extracted and with PCR transgenic fish were identified thanks to the gene encoding the protein DsRed (D).
B. Riluzole treatment significantly reduced the frequency of spontaneous tail coilings, the percentage of multiple coilings and the percentage of embryos performing multiple and complex coilings both in Ctrl and mSod1 embryos. In the case of mSod1 embryos, the frequency of spontaneous coiling, the percentage of multiple tail coilings and the type of multiple tail coilings (the relative percentage of alternating and same side tail bends) were brought to levels comparable to those of Ctrl embryos before riluzole administration. Columns in each graph represent mean ± SEM of the indicated parameter, calculated in 28 Ctrl and 23 mSod1 embryos before and after riluzole treatment. Measures were statistically analyzed with unpaired Student t test. Means were considered statistically different when $P < 0.05$.
C. Riluzole treatment did not affect motor axons morphology of Ctrl embryos; however, it significantly increased motor axons length in mSod1 embryos. Columns in each graph represent mean ± SEM of the indicated parameter, calculated in Ctrl and mSod1 embryos not incubated (28 and 33 respectively) or incubated with riluzole solution (10 and 22 respectively). Measures were statistically analyzed with unpaired Student t test. Means were considered statistically different when $P < 0.05$.

(*, $P < 0.05$; **, $P < 0.01$; ***, $P < 0.001$; ****, $P < 0.0001$)

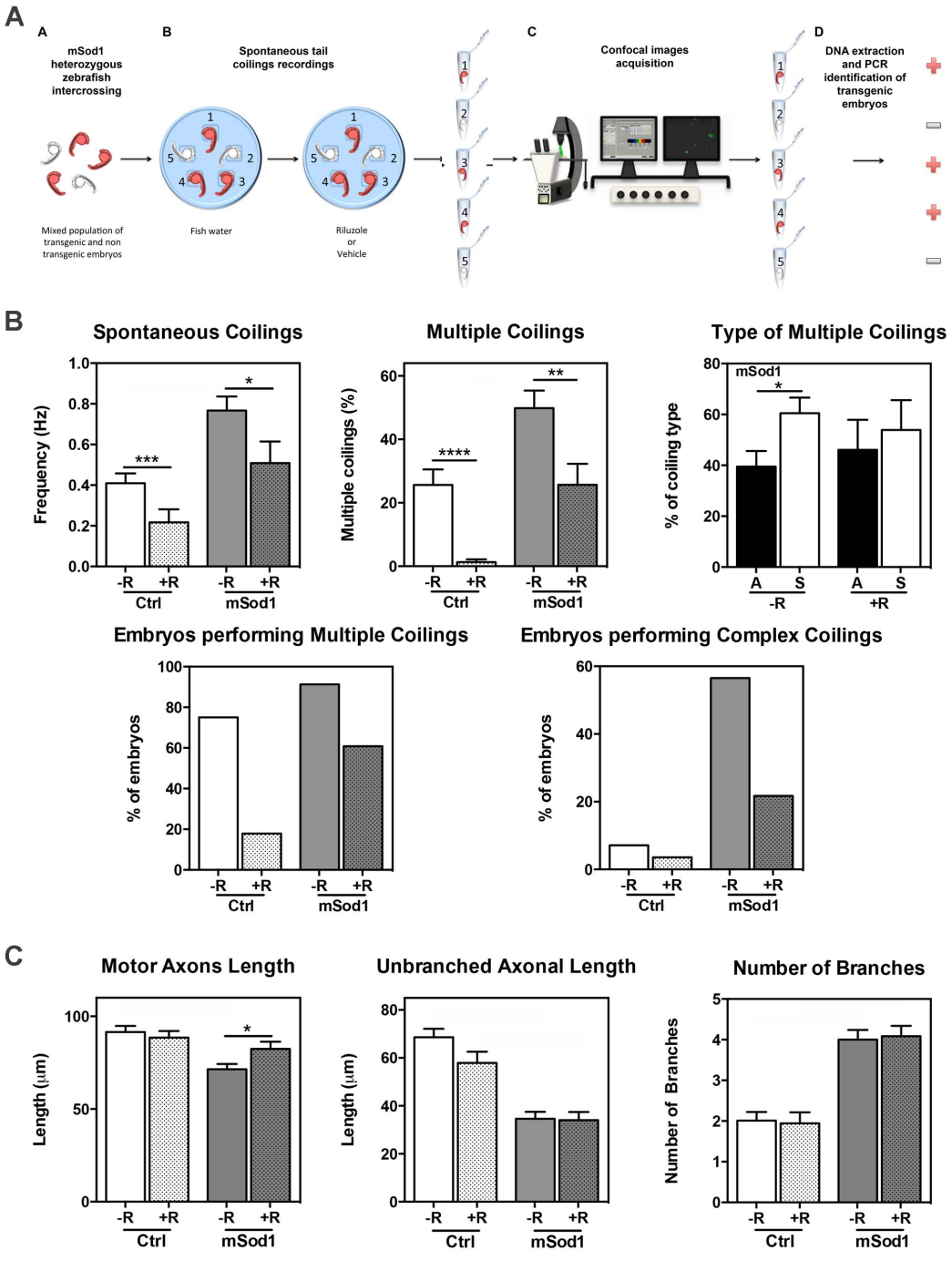
A
A
mSod1 heterozygous zebrafish intercrossing
Mixed population of transgenic and non transgenic embryos
B
Spontaneous tail coilings recordings
Fish water
Riluzole or Vehicle
C
Confocal images acquisition
D
DNA extraction and PCR identification of transgenic embryos
B
Spontaneous Coilings
Frequency (Hz)
Multiple Coilings
Multiple coilings (%)
Type of Multiple Coilings
% of coiling type
mSod1
A
S
Embryos performing Multiple Coilings
% of embryos
Embryos performing Complex Coilings
% of embryos
-R
+R
Ctrl
mSod1
C
Motor Axons Length
Length (µm)
Unbranched Axonal Length
Length (µm)
Number of Branches
Number of Branches

FIGURE 16: mSod1 spinal motor neurons show more frequent spontaneous depolarizations

A. To test whether the aberrant motor phenotype observed in mSod1 embryos at 20 hpf, was associated to alterations in the spontaneous depolarizations of spinal neurons, in the intact spinal network, we microinjected one-cell stage embryos with the FRET-based voltage biosensor Mermaid under the control of the pan-neuronal promoter HuC. The bright field image, merged with the fluorescence signal, shows the efficient expression of the biosensor in an individual motor neuron. Beside, the donor and FRET channel detected are shown. Scale bar: 10 μm.
B. FRET Ratio map showing the FRET Ratio calculated in a motor neuron during a spontaneous depolarization (indicated with a red line in the FRET ratio graph in panel C). Scale bar: 10 μm.
C. These plots show representative examples of the spontaneous mean FRET Ratio changes in a Ctrl and in a mSod1 motor neuron during a one minute recording. For this biosensor, the increase in FRET Ratio happens when the membrane potential increases. In the inset, the detailed morphology of 2 depolarization events are shown.
D. In mSod1 motor neurons we measured a significant increase in the frequency of spontaneous depolarizations but no changes in the FRET basal ratio or in the amplitude and duration of depolarizations compared to Ctrl embryos motor neurons. Columns in each graph represent mean ± SEM of the indicated parameter, calculated in 12 Ctrl and 12 mSod1 motor neurons. Measures were statistically analyzed with unpaired Student t test. Means were considered statistically different when $P < 0.05$. (***, $P < 0.001$)

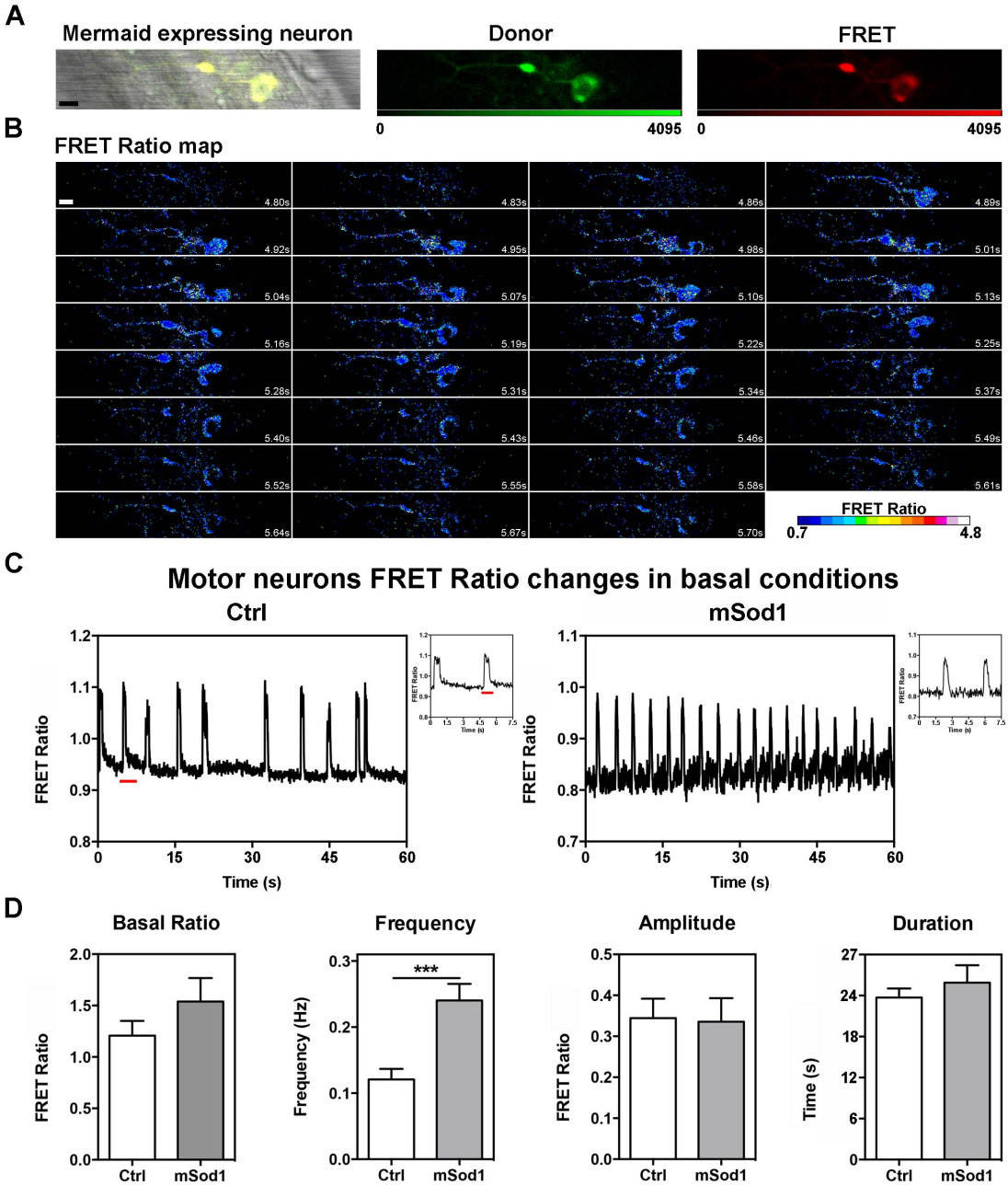
A
Mermaid expressing neuron
Donor
FRET
0
4095
0
4095
B
FRET Ratio map
FRET Ratio
0.7
4.8
C
Motor neurons FRET Ratio changes in basal conditions
Ctrl
mSod1
FRET Ratio
Time (s)
D
Basal Ratio
Frequency
Amplitude
Duration
Frequency (Hz)
Time (s)
***
Ctrl
mSod1

FIGURE 17: Riluzole administration decreases the frequency of spinal motor neurons spontaneous depolarizations

A. These plots display representative traces showing the FRET Ratio changes recorded in the same Ctrl and mSod1 motor neuron before and after 5 minutes of riluzole administration.
B. The statistical analyses showed that riluzole did not affect motor neurons FRET basal ratio and amplitude and duration of periodic depolarizations but significantly reduced the frequency of depolarization events in both Ctrl and mSod1 motor neurons. In particular, after riluzole treatment, mSod1 motor neurons undergo to spontaneous depolarization with a frequency comparable to that of Ctrl motor neurons before riluzole treatment. Histograms columns in each graph represent mean ± SEM of the indicated parameter, calculated in 12 Ctrl and 12 mSod1 motor neurons. Measures were statistically analyzed with unpaired Student t test. Means were considered statistically different when $P < 0.05$.
(*, $P < 0.05$; **, $P < 0.01$)

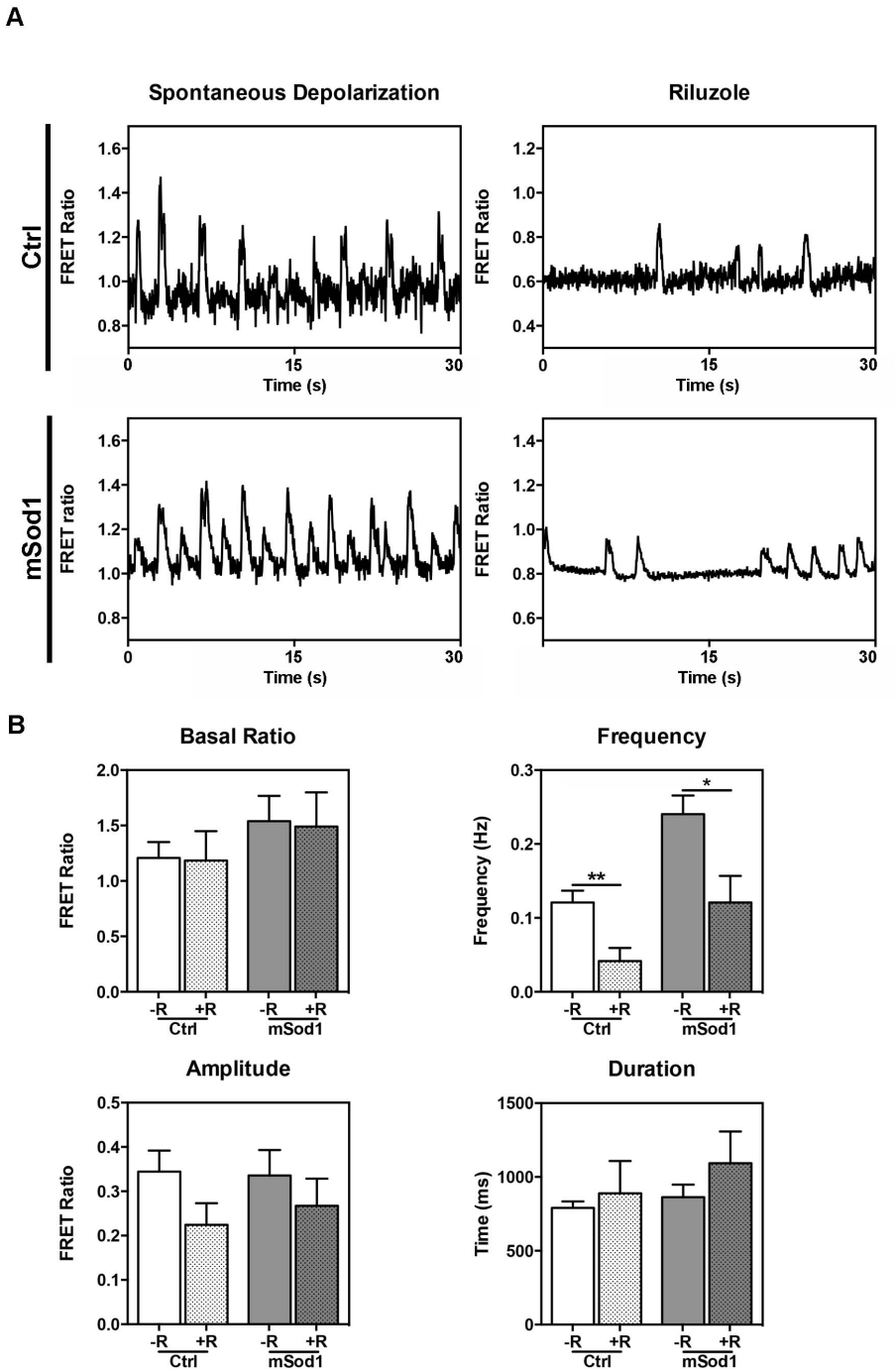
A
Spontaneous Depolarization
Riluzole
Ctrl
mSod1
FRET Ratio
FRET ratio
Time (s)
B
Basal Ratio
Frequency
Amplitude
Duration
Frequency (Hz)
Time (ms)
-R
+R
Ctrl
mSod1
**
*

FIGURE 18: Spinal interneurons present different patterns of membrane voltage changes and differently respond to riluzole treatment

We recorded membrane voltage changes in Ctrl and mSod1 embryos interneurons at 20 hpf. In both cases, we identified 3 different classes of interneurons exhibiting different electrical properties. A subtype of interneurons does not show periodic depolarizations and does not change its depolarization features after riluzole administration (Type 0); a group of interneurons presents periodic depolarizations in basal condition and reduces its frequency after riluzole treatment (Type 1) and a class of interneurons develops periodic depolarizations only after riluzole incubation (Type 2).

A. This panel shows representative examples of FRET Ratio changes, recorded before and after riluzole administration, in 3 interneurons belonging to the 3 different classes described above in Ctrl embryos.
   Most interneurons (66%) do not show periodic depolarization and their electrical properties do not change after riluzole treatment (Type 0). The remaining interneurons display periodic depolarizations before riluzole incubation in the 75% of cases (Type 1) and only after riluzole administration in the 25% of cases (Type 2).
B. This panel presents representative examples of FRET Ratio changes recorded in 3 mSod1 embryos spinal interneurons, representative of the 3 different classes described, before and after riluzole incubation.
   Also in mSod1 embryos, most interneurons (67%) do not show periodic depolarizations either before or after riluzole treatment (Type 0). Other interneurons undergo to periodic depolarization before riluzole incubation in the 73% of cases and only after riluzole administration in the 27% of cases (Type 2).

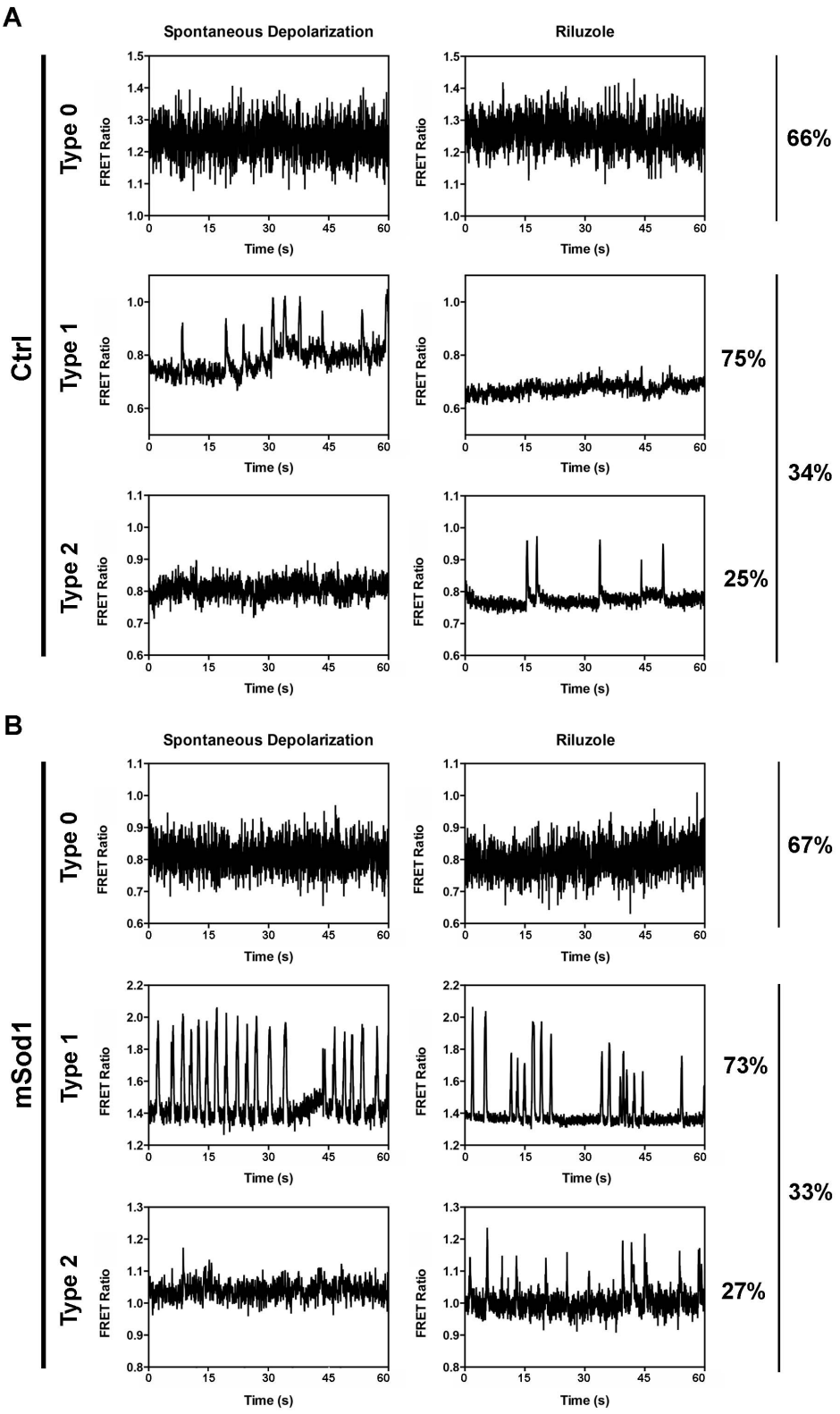
A
Spontaneous Depolarization
Riluzole
Ctrl
Type 0
Type 1
Type 2
FRET Ratio
Time (s)
66%
75%
25%
34%
B
Spontaneous Depolarization
Riluzole
mSod1
Type 0
Type 1
Type 2
FRET Ratio
Time (s)
67%
73%
27%
33%

FIGURE 19: mSod1 embryos spinal interneurons show more frequent spontaneous depolarizations that decrease after riluzole treatment

A. This panel compares basal FRET ratio and spontaneous depolarizations frequency recorded in motor neurons (Mn) and interneurons (In) in Ctrl and mSod1 embryos spinal cord. We did not detect any differences in the basal ratio measured in motor neurons and Type 1 interneurons either before (-R) or after (+R) riluzole treatment, both in Ctrl and mSod1 embryos. Also the frequency of spontaneous depolarizations and its reduction after riluzole treatment is comparable between motor neurons and interneurons in Ctrl and mSod1 embryos.
B. This panel shows the basal FRET ratio and the frequency of spontaneous depolarizations recorded in Type 1 and Type 2 interneurons in Ctrl and mSod1 embryos. Ctrl and mSod1 Type 1 interneurons do not show differences in their basal FRET ratio before riluzole treatment and do not change their basal ratio after the drug administration. mSod1 Type 1 interneurons present a significant higher frequency of spontaneous depolarizations compared to that of Ctrl embryos. Both in the case of Ctrl and mSod1 Type1 interneurons, riluzole significantly reduces the frequency of spontaneous depolarizations. Type 2 interneurons do not display significant differences in the basal FRET ratio in mSod1 embryos compared to Ctrl before and after riluzole administration; however, riluzole treatment causes the comparison of spontaneous depolarizations at comparable frequency in Ctrl and mSod1 interneurons.
C. We did not measure any differences in the amplitude and durations of spontaneous depolarizations in Ctrl and mSod1 Type 1 interneurons before and after riluzole treatment.

Columns in each graph represent mean ± SEM of the indicated parameter. Measures were statistically analyzed with unpaired Student t test. Means were considered statistically different when $P < 0.05$.
(*, $P < 0.05$; **, $P<0.01$)

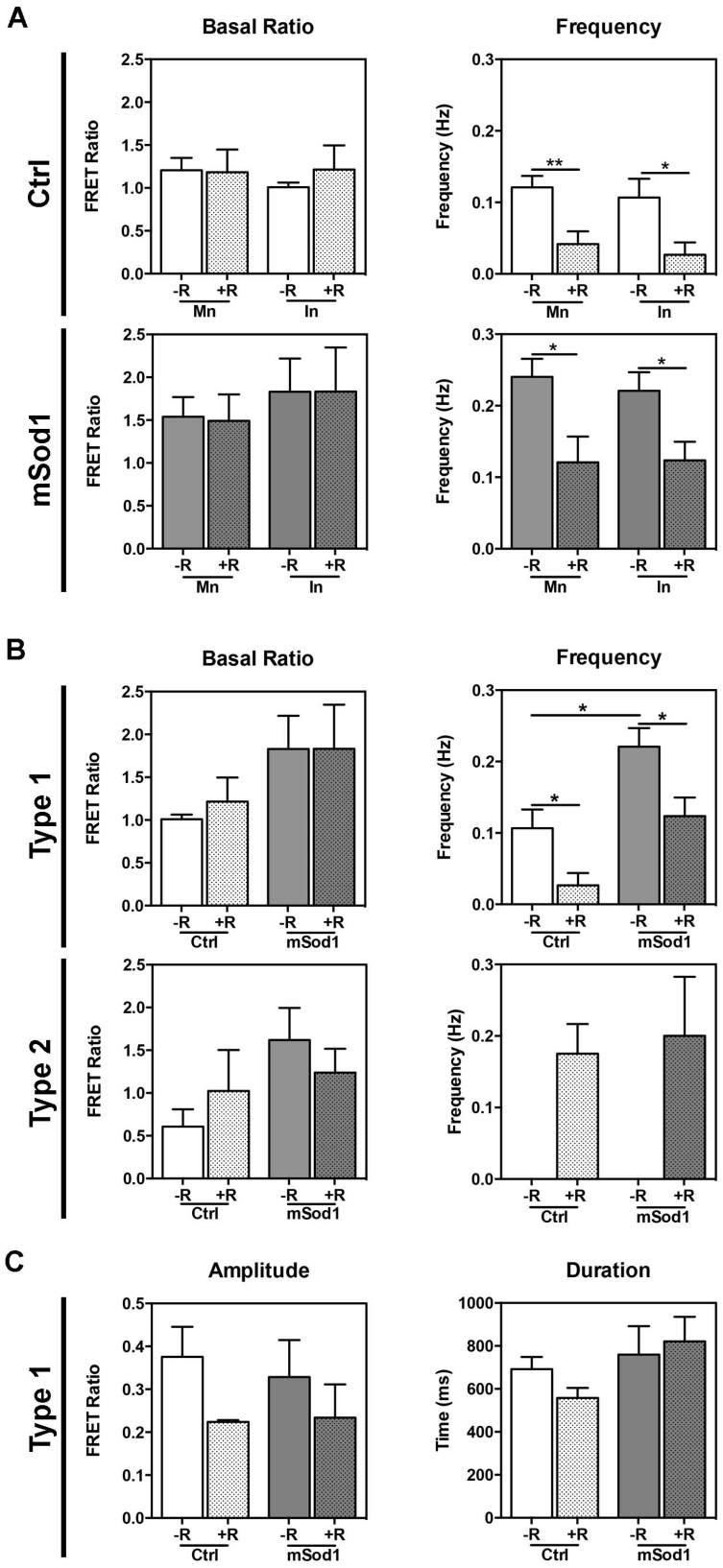
A
Basal Ratio
Frequency
Ctrl
mSod1
FRET Ratio
Frequency (Hz)
-R
+R
Mn
In
B
Type 1
Type 2
Ctrl
mSod1
C
Amplitude
Duration
Time (ms)

REFERENCES

Ajroud-Driss S, Siddique T. **Sporadic and hereditary amyotrophic lateral sclerosis (ALS).** *Biochim Biophys Acta*. 2014 Sep 1.

Alexianu ME, Kozovska M, Appel SH. **Immune reactivity in a mouse model of familial ALS correlates with disease progression.** *Neurology*. 2001 Oct 9;57(7):1282-9.

Amendola J, Durand J. **Morphological differences between wild-type and transgenic superoxide dismutase 1 lumbar motoneurons in postnatal mice.** *J Comp Neurol*. 2008 Nov 20;511(3):329-41.

Ampatzis K, Song J, Ausborn J, El Manira A. **Pattern of innervation and recruitment of different classes of motoneurons in adult zebrafish.** *J Neurosci.* 2013 Jun 26;33(26):10875-86.

Andersen PM. **Amyotrophic lateral sclerosis associated with mutations in the CuZn superoxide dismutase gene.** *Curr Neurol Neurosci Rep*. 2006 Jan;6(1):37-46.

Andersen PM, Al-Chalabi A. **Clinical genetics of amyotrophic lateral sclerosis: what do we really know?** *Nat Rev Neurol*. 2011 Oct 11;7(11):603-15.

Armstrong GA, Drapeau P. **Loss and gain of FUS function impair neuromuscular synaptic transmission in a genetic model of ALS.** *Hum Mol Genet*. 2013 Nov 1;22(21):4282-92.

Babin PJ, Goizet C, Raldúa D. **Zebrafish models of human motor neuron diseases: advantages and limitations.** *Prog Neurobiol*. 2014 Jul;118:36-58.

Bahadorani S, Mukai ST, Rabie J, Beckman JS, Phillips JP, Hilliker AJ. **Expression of zinc-deficient human superoxide dismutase in Drosophila neurons produces a locomotor defect linked to mitochondrial dysfunction.** *Neurobiol Aging*. 2013 Oct;34(10):2322-30.

Bellingham MC. **A review of the neural mechanisms of action and clinical efficiency of riluzole in treating amyotrophic lateral sclerosis: what have we learned in the last decade?** *CNS Neurosci Ther*. 2011 Feb;17(1):4-31.

Bensimon G, Lacomblez L, Meininger V. **A controlled trial of riluzole in amyotrophic lateral sclerosis. ALS/Riluzole Study Group.** *N Engl J Med*. 1994 Mar 3;330(9):585-91.

Boillée S, Yamanaka K, Lobsiger CS, Copeland NG, Jenkins NA, Kassiotis G, Kollias G, Cleveland DW. **Onset and progression in inherited ALS determined by motor neurons and microglia.** *Science*. 2006 Jun 2;312(5778):1389-92.

Bolte S, Cordelières FP. **A guided tour into subcellular colocalization analysis in light microscopy.** *J Microsc*. 2006 Dec;224(Pt 3):213-32.

Boyer JG, Ferrier A, Kothary R. **More than a bystander: the contributions of intrinsic skeletal muscle defects in motor neuron diseases**. *Front Physiol*. 2013 Dec 18;4:356.

Bosco DA, Morfini G, Karabacak NM, Song Y, Gros-Louis F, Pasinelli P, Goolsby H, Fontaine BA, Lemay N, McKenna-Yasek D, Frosch MP, Agar JN, Julien JP, Brady ST, Brown RH Jr. **Wild-type and mutant SOD1 share an aberrant conformation and a common pathogenic pathway in ALS.** *Nat Neurosci*. 2010 Nov;13(11):1396-403.

Brustein E, Saint-Amant L, Buss RR, Chong M, McDearmid JR, Drapeau P. **Steps during the development of the zebrafish locomotor network.** *J Physiol Paris*. 2003 Jan;97(1):77-86.

Cappello V, Vezzoli E, Righi M, Fossati M, Mariotti R, Crespi A, Patruno M, Bentivoglio M, Pietrini G, Francolini M. **Analysis of neuromuscular junctions and effects of anabolic steroid administration in the SOD1G93A mouse model of ALS.** *Mol Cell Neurosci*. 2012 Aug;51(1-2):12-21.

Casci I, Pandey UB. **A fruitful endeavor: Modeling ALS in the fruit fly.** Brain Res. 2014 Oct 5. pii: S0006-8993(14)01337-7. doi: 10.1016/j.

Chiu IM, Phatnani H, Kuligowski M, Tapia JC, Carrasco MA, Zhang M, Maniatis T, Carroll MC. **Activation of innate and humoral immunity in the peripheral nervous system of ALS transgenic mice.** *Proc Natl Acad Sci U S A*. 2009 Dec 8;106(49):20960-5.

Chiu AY, Zhai P, Dal Canto MC, Peters TM, Kwon YW, Prattis SM, Gurney ME**. Age-dependent penetrance of disease in a transgenic mouse model of familial amyotrophic lateral sclerosis.** *Mol Cell Neurosci*. 1995 Aug;6(4):349-62.

Ciura S, Lattante S, Le Ber I, Latouche M, Tostivint H, Brice A, Kabashi E. **Loss of function of C9orf72 causes motor deficits in a zebrafish model of amyotrophic lateral sclerosis.** *Ann Neurol*. 2013 Aug;74(2):180-7.

Clement AM, Nguyen MD, Roberts EA, Garcia ML, Boillee S, Rule M, et al. **Wild-type non neuronal cells extend survival of SOD1 mutant motor neurons in ALS mice**. *Science.* 2003;302: 113–117.

Dal Canto MC, Gurney ME. **Neuropathological changes in two lines of mice carrying a transgene for mutant human Cu,Zn SOD, and in mice overexpressing wild type human SOD: a model of familial amyotrophic lateral sclerosis (FALS).** *Brain Res.* 1995 Apr 3;676(1):25-40.

Da Costa MM, Allen CE, Higginbottom A, Ramesh T, Shaw PJ, McDermott CJ. **A new zebrafish model produced by TILLING of SOD1-related amyotrophic lateral sclerosis replicates key features of the disease and represents a tool for in vivo therapeutic screening.** *Dis Model Mech*. 2014 Jan;7(1):73-81.

De Vos KJ, Chapman AL, Tennant ME, Manser C, Tudor EL, Lau KF, Brownlees J, Ackerley S, Shaw PJ, McLoughlin DM, Shaw CE, Leigh PN, Miller CC,Grierson AJ. **Familial amyotrophic lateral sclerosis-linked SOD1 mutants perturb fast axonal transport to reduce axonal mitochondria content**. *Hum Mol Genet*. 2007 Nov 15;16(22):2720-8.

Drapeau P, Saint-Amant L, Buss RR, Chong M, McDearmid JR, Brustein E. **Development of the locomotor network in zebrafish.** *Prog Neurobiol.* 2002 Oct;68(2):85-111.

Dobrowolny G, Aucello M, Rizzuto E, Beccafico S, Mammucari C, Boncompagni S, Belia S, Wannenes F, Nicoletti C, Del Prete Z, Rosenthal N, Molinaro M,Protasi F, Fanò G, Sandri M, Musarò A. **Skeletal muscle is a primary target of SOD1G93A-mediated toxicity.** *Cell Metab*. 2008 Nov;8(5):425-36.

Dupuis L, di Scala F, Rene F, de Tapia M, Oudart H, Pradat PF, Meininger V, Loeffler JP. **Up-regulation of mitochondrial uncoupling protein 3 reveals an early muscular metabolic defect in amyotrophic lateral sclerosis.** *FASEB J*. 2003 Nov;17(14):2091-3.

Durazo A, Shaw BF, Chattopadhyay M, Faull KF, Nersissian AM, Valentine JS, Whitelegge JP**. Metal-free superoxide dismutase-1 and three different amyotrophic lateral sclerosis variants share a similar partially unfolded beta-barrel at physiological temperature.** *J Biol Chem*. 2009 Dec 4;284(49):34382-9.

Eisen A, Weber M. **Neurophysiological evaluation of cortical function in the early diagnosis of ALS.** *Amyotroph Lateral Scler Other Motor Neuron Disord*. 2002; 1:S47-S51.

Elshafey A, Lanyon WG, Connor JM. **Identification of a new missense point mutation in exon 4 of the Cu/Zn superoxide dismutase (SOD-1) gene in a family with amyotrophic lateral sclerosis.** *Hum Mol Genet*. 1994 Feb;3(2):363-4.

Ferraiuolo L, Kirby J, Grierson AJ, Sendtner M, Shaw PJ. **Molecular pathways of motor neuron injury in amyotrophic lateral sclerosis.** *Nat Rev Neurol*. 2011 Nov;7(11):616-30.

Filipchuk AA, Durand J. **Postnatal dendritic development in lumbar motoneurons in mutant superoxide dismutase 1 mouse model of amyotrophic lateral sclerosis.** *Neuroscience*. 2012 May 3;209:144-54

Fischer LR, Culver DG, Tennant P, Davis AA, Wang M, Castellano-Sanchez A, Khan J, Polak MA, Glass JD. **Amyotrophic lateral sclerosis is a distal axonopathy: evidence in mice and man.** *Exp Neurol*. 2004 Feb;185(2):232-40.

Frey D, Schneider C, Xu L, Borg J, Spooren W, Caroni P. **Early and selective loss of neuromuscular synapse subtypes with low sprouting competence in motoneuron diseases.** *J Neurosci.* 2000 Apr 1;20(7):2534-42.

Gould TW, Buss RR, Vinsant S, Prevette D, Sun W, Knudson CM, Milligan CE, Oppenheim RW. **Complete dissociation of motor neuron death from motor dysfunction by Bax deletion in a mouse model of ALS.** *J Neurosci*. 2006 Aug 23;26(34):8774-86.

Guo H, Lai L, Butchbach ME, Stockinger MP, Shan X, Bishop GA, Lin CL. **Increased expression of the glial glutamate transporter EAAT2 modulates excitotoxicity and delays the onset but not the outcome of ALS in mice.** *Hum Mol Genet*. 2003 Oct 1;12(19):2519-32.

Gurney ME, Pu H, Chiu AY, Dal Canto MC, Polchow CY, Alexander DD, Caliendo J, Hentati H, Kwon YW, Deng H, Chen W, Zhai P, Sufit RL, Siddique T. **Motor neuron degeneration in mice that express a human Cu/Zn superoxide dismutase mutation.** *Science*. 1994;264:1772–5.

Habib AA, Mitsumoto H**. Emerging drugs for amyotrophic lateral sclerosis.** *Expert Opin Emerg Drugs*. 2011 Sep;16(3):537-58.

Hegedus J, Putman CT, Tyreman N, Gordon T. **Preferential motor unit loss in the SOD1 G93A transgenic mouse model of amyotrophic lateral sclerosis.** *J Physiol*. 2008 Jul 15;586(14):3337-51.

Hodgson L, Shen F, Hahn K. **Biosensors for characterizing the dynamics of rho family GTPases in living cells.** *Curr Protoc Cell Biol*. 2010; Chapter 14:Unit 14.11.1-26.

Huang SH, Hsiao CD, Lin DS, Chow CY, Chang CJ, Liau I. **Imaging of zebrafish in vivo with second-harmonic generation reveals shortened sarcomeres associated with myopathy induced by statin.** *PLoS One*. 2011;6(9):e24764.

Islam R, Kumimoto EL, Bao H, Zhang B. **ALS-linked SOD1 in glial cells enhances ß-N-Methylamino L-Alanine (BMAA)-induced toxicity in Drosophila.** *F1000Res*. 2012 Nov 9;1:47. doi: 10.12688/f1000research.1-47.v1. *eCollection 2012*.

Jaarsma D. **Swelling and vacuolisation of mitochondria in transgenic SOD1-ALS mice: a consequence of supranormal SOD1 expression?** Mitochondrion. 2006 Feb;6(1):48-9; author reply 50-1.

Johnson JO, Pioro EP, Boehringer A, Chia R, Feit H, Renton AE, Pliner HA, Abramzon Y, Marangi G, Winborn BJ, Gibbs JR, Nalls MA, Morgan S, Shoai M, Hardy J, Pittman A, Orrell RW, Malaspina A, Sidle KC, Fratta P, Harms MB, Baloh RH, Pestronk A, Weihl CC, Rogaeva E, Zinman L, Drory VE, Borghero G, Mora G, Calvo A, Rothstein JD; ITALSGEN Consortium, Drepper C, Sendtner M, Singleton AB, Taylor JP, Cookson MR, Restagno G, Sabatelli M, Bowser R, Chiò A, Traynor BJ. **Mutations in the Matrin 3 gene cause familial amyotrophic lateral sclerosis.** *Nat Neurosci*. 2014 May;17(5):664-6.

Joyce PI, Fratta P, Fisher EM, Acevedo-Arozena A. **SOD1 and TDP-43 animal models of amyotrophic lateral sclerosis: recent advances in understanding disease toward the development of clinical treatments.** *Mamm Genome*. 2011;22:420–48.

Kabashi E, Bercier V, Lissouba A, Liao M, Brustein E, Rouleau GA, Drapeau P. **FUS and TARDBP but not SOD1 interact in genetic models of amyotrophic lateral sclerosis**. *PLoS Genet*. 2011 Aug;7(8): e1002214.

Kabashi E, Champagne N, Brustein E, Drapeau P. **In the swim of things: recent insights to neurogenetic disorders from zebrafish.** *Trends Genet.* 2010 Aug;26(8):373-81. (a)

Kabashi E, El Oussini H, Bercier V, Gros-Louis F, Valdmanis PN, McDearmid J, Mejier IA, Dion PA, Dupre N, Hollinger D, Sinniger J, Dirrig-Grosch S, Camu W,Meininger V, Loeffler JP, René F, Drapeau P, Rouleau GA, Dupuis L. **Investigating the contribution of VAPB/ALS8 loss of function in amyotrophic lateral sclerosis.** *Hum Mol Genet.* 2013 Jun 15;22(12):2350-60.

Kabashi E, Lin L, Tradewell ML, Dion PA, Bercier V, Bourgouin P, Rochefort D, Bel Hadj S, Durham HD, Van de Velde C, Rouleau GA, Drapeau P. **Gain and loss of function of ALS-related mutations of TARDBP (TDP-43) cause motor deficits in vivo.** *Hum Mol Genet*. 2010 Dec;19(4):671–683. (b)

Kalueff AV, Gebhardt M, Stewart AM, Cachat JM, Brimmer M, Chawla JS, Craddock C, Kyzar EJ, Roth A, Landsman S, Gaikwad S, Robinson K, Baatrup E, Tierney K, Shamchuk A, Norton W, Miller N, Nicolson T, Braubach O, Gilman CP, Pittman J, Rosemberg DB, Gerlai R, Echevarria D, Lamb E, Neuhauss SC, Weng W, Bally-Cuif L, Schneider H; Zebrafish Neuroscience Research Consortium. **Towards a comprehensive catalog of zebrafish behavior 1.0 and beyond.** *Zebrafish.* 2013 Mar;10(1):70-86.

Kanai K, Shibuya K, Sato Y, Misawa S, Nasu S, Sekiguchi Y, Mitsuma S, Isose S, Fujimaki Y, OhmoriS, Koga S, Kuwabara S**. Motor axonal excitability properties are strong predictors for survival in amyotrophic lateral sclerosis.** *J Neurol Neurosurg Psychiatry*. 2012 Jul;83(7):734-8.

Kato S. **Amyotrophic lateral sclerosis models and human neuropathology: similarities and differences.** *Acta Neuropathol*. 2008 Jan;115(1):97-114.

Kawamata T, Akiyama H, Yamada T, McGeer PL. **Immunologic reactions in amyotrophic lateral sclerosis brain and spinal cord tissue.** *Am. J. Pathol*. 1992 140, 691–707.

Keller AF, Gravel M, Kriz J. **Live imaging of amyotrophic lateral sclerosis pathogenesis: disease onset is characterized by marked induction of GFAP in Schwann cells.** *Glia*. 2009 Aug 1;57(10):1130-42.

Kiernan MC, Vucic S, Cheah BC, Turner MR, Eisen A, Hardiman O, Burrell JR, Zoing MC. **Amyotrophic lateral sclerosis.** *Lancet*. 2011 Mar 12;377(9769).

Kimmel CB, Ballard WW, Kimmel SR, Ullmann B, Schilling TF. **Stages of embryonic development of the zebrafish.** *Dev Dyn*. 1995 Jul;203(3):253-310.

Knogler LD, Ryan J, Saint-Amant L, Drapeau P. **A hybrid electrical/chemical circuit in the spinal cord generates a transient embryonic motor behavior.** *J Neurosci*. 2014 Jul 16;34(29):9644-55.

Kuo JJ, Schonewille M, Siddique T, Schults AN, Fu R, Bar PR, Anelli R, Heckman CJ, Kroese AB. **Hyperexcitability of cultured spinal motorneurons from presyntomatic ALS mice.** *J Neurophysiol*. 2004; 91:571-575.

Kuo JJ, Siddique T, Fu R, Heckman CJ. **Increased persistent Na(+) current and its effect on excitability in motoneurones cultured from mutant SOD1 mice.** *J Physiol*. 2005; 563:843-854.

Lai C, Xie C, McCormack SG, Chiang HC, Michalak MK, Lin X, Chandran J, Shim H, Shimoji M, Cookson MR, Huganir RL, Rothstein JD, Price DL, Wong PC, Martin LJ, Zhu JJ, Cai H. **Amyotrophic lateral sclerosis 2-deficiency leads to neuronal degeneration in amyotrophic lateral sclerosis through altered AMPA receptor trafficking.** *J Neurosci*. 2006 Nov 8;26(45):11798-806.

Lemmens R, Van Hoecke A, Hersmus N, Geelen V, D'Hollander I, Thijs V, Van Den Bosch L, Carmeliet P, Robberecht W. **Overexpression of mutant superoxide dismutase 1 causes a motor axonopathy in the zebrafish.** *Hum Mol Genet.* 2007 Oct 1;16(19):2359-65.

Lepore AC, Rauck B, Dejea C, Pardo AC, Rao MS, Rothstein JD, Maragakis NJ. **Focal transplantation-based astrocyte replacement is neuroprotective in a model of motor neuron disease.** *Nat Neurosci*. 2008 Nov;11(11):1294-301.

Lewis KE, Eisen JS. **From cells to circuits: development of the zebrafish spinal cord.** *Prog Neurobiol.* 2003 Apr;69(6):419-49.

Li J, Li T, Zhang X, Tang Y, Yang J, Le W. **Human superoxide dismutase 1 overexpression in motor neurons of Caenorhabditis elegans causes axon guidance defect and neurodegeneration.** *Neurobiol Aging*. 2014 Apr;35(4):837-46.

Ling SC, Polymenidou M, Cleveland DW. **Converging mechanisms in ALS and FTD: disrupted RNA and protein homeostasis.** *Neuron*. 2013 Aug 7;79(3):416-38.

Lino MM, Schneider C, Caroni P. **Accumulation of SOD1 mutants in postnatal motoneurons does not cause motoneuron pathology or motoneuron disease.** *J Neurosci*. 2002;22: 4825– 4832.

Mackenzie IR, Rademakers R, Neumann M. **TDP-43 and FUS in amyotrophic lateral sclerosis and frontotemporal dementia.** *Lancet Neurol*. 2010 Oct;9(10):995-1007.

Mahoney DJ, Kaczor JJ, Bourgeois J, Yasuda N, Tarnopolsky MA. **Oxidative stress and antioxidant enzyme upregulation in SOD1-G93A mouse skeletal muscle.** *Muscle Nerve.* 2006 Jun;33(6):809-16.

Martin E, Cazenave W, Cattaert D, Branchereau P. **Embryonic alteration of motoneuronal morphology induces hyperexcitability in the mouse model of amyotrophic lateral sclerosis.** *Neurobiol Dis.* 2013 Jun;54:116-26.

Matthews M, Varga ZM. **Anesthesia and euthanasia in zebrafish.** *ILAR J.* 2012;53(2):192-204. doi: 10.1093/ilar.53.2.192.

McGown A, McDearmid JR, Panagiotaki N, Tong H, Al Mashhadi S, Redhead N, Lyon AN, Beattie CE, Shaw PJ, Ramesh TM. **Early interneuron dysfunction in ALS: insights from a mutant sod1 zebrafish model.** *Ann Neurol*. 2013 Feb;73(2):246-58.

Menon P, Kiernan MC, Vucic S. **Cortical hyperexcitability precedes lower motor neuron dysfunction in ALS.** *Clin Neurophysiol.* 2014 Aug 28. pii: S1388-2457(14)00414-3. doi: 10.1016/j.clinph.2014.04.023.

Mori K, Lammich S, Mackenzie IR, Forné I, Zilow S, Kretzschmar H, Edbauer D, Janssens J, Kleinberger G, Cruts M, Herms J, Neumann M, Van Broeckhoven C, Arzberger T, Haass C**. hnRNP A3 binds to GGGGCC repeats and is a constituent of p62-positive/TDP43-negative inclusions in the hippocampus of patients with C9orf72 mutations.** *Acta Neuropathol*. 2013 Mar;125(3):413-23.

Nagy D, Kato T, Kushner PD. **Reactive astrocytes are widespread in the cortical gray matter of amyotrophic lateral sclerosis.** *J Neurosci Res.* 1994 Jun 15;38(3):336-47.

Oeda T, Shimohama S, Kitagawa N, Kohno R, Imura T, Shibasaki H, Ishii N. **Oxidative stress causes abnormal accumulation of familial amyotrophic lateral sclerosis-related mutant SOD1 in transgenic Caenorhabditis elegans.** *Hum Mol Genet.* 2001 Sep 15;10(19):2013-23.

Orrell RW, Habgood JJ, Malaspina A, Mitchell J, Greenwood J, Lane RJ, de Belleroche JS. **Clinical characteristics of SOD1 gene mutations in UK families with ALS.** *J Neurol Sci*. 1999 Oct 31;169(1-2):56-60.

Panzer JA, Gibbs SM, Dosch R, Wagner D, Mullins MC, Granato M, Balice-Gordon RJ. **Neuromuscular synaptogenesis in wild-type and mutant zebrafish**. *Dev Biol*. 2005 Sep 15;285(2):340-57.

Pardo AC, Wong V, Benson LM, Dykes M, Tanaka K, Rothstein JD, Maragakis NJ. **Loss of the astrocyte glutamate transporter GLT1 modifies disease in SOD1(G93A) mice.** *Exp Neurol*. 2006 Sep;201(1):120-30.

Parichy DM, Elizondo MR, Mills MG, Gordon TN, Engeszer RE. **Normal table of postembryonic zebrafish development: staging by externally visible anatomy of the living fish.** *Dev Dyn*. 2009 Dec;238(12):2975-3015. doi: 10.1002/dvdy.22113.

Park HC, Kim CH, Bae YK, Yeo SY, Kim SH, Hong SK, Shin J, Yoo KW, Hibi M, Hirano T, Miki N, Chitnis AB, Huh TL. **Analysis of upstream elements in the HuC promoter leads to the establishment of transgenic zebrafish with fluorescent neurons.** *Dev Biol.* 2000 Nov 15;227(2):279-93.

Philips T, Rothstein JD. **Glial cells in amyotrophic lateral sclerosis.** *Exp Neurol*. 2014 May 22. pii: S0014-4886(14)00157-5. doi: 10.1016/j.expneurol.2014.05.015.

Pieri M, Carunchio I, Curcio L, Mercuri NB, Zona C. **Increased persistent sodium current determines cortical hyperexcitability in a genetic model of amyotrophic lateral sclerosis.** *Exp Neurol.* 2009 Feb;215(2):368-79.

Pramatarova A, Laganiere J, Roussel J, Brisebois K, Rouleau GA. **Neuron-specific expression of mutant superoxide dismutase 1 in transgenic mice does not lead to motor impairment.** *J Neurosci*. 2001;21:3369–3374.

Pun S, Santos AF, Saxena S, Xu L, Caroni P. **Selective vulnerability and pruning of phasic motoneuron axons in motoneuron disease alleviated by CNTF.** *Nat Neurosci.* 2006 Mar;9(3):408-19. Epub 2006 Feb 12.

Ramesh T, Lyon AN, Pineda RH, Wang C, Janssen PM, Canan BD, Burghes AH, Beattie CE. **A genetic model of amyotrophic lateral sclerosis in zebrafish displays phenotypic hallmarks of motoneuron disease**. *Dis Model Mech*. 2010 Sept-Oct;3(9-10):652-62.

Reaume AG, Elliott JL, Hoffman EK, Kowall NW, Ferrante RJ, Siwek DF, Wilcox HM, Flood DG, Beal MF, Brown RH Jr, Scott RW, Snider WD. **Motor neurons in Cu/Zn superoxide dismutase-deficient mice develop normally but exhibit enhanced cell death after axonal injury.** *Nat Genet*. 1996 May;13(1):43-7.

Renton AE, Chiò A, Traynor BJ. **State of play in amyotrophic lateral sclerosis genetics.** *Nat Neurosci*. 2014 Jan;17(1):17-23.

Renton AE, Majounie E, Waite A, Simón-Sánchez J, Rollinson S, Gibbs JR, Schymick JC, Laaksovirta H, van Swieten JC, Myllykangas L, Kalimo H, Paetau A, Abramzon Y, Remes AM, Kaganovich A, Scholz SW, Duckworth J, Ding J, Harmer DW, Hernandez DG, Johnson JO, Mok K, Ryten M, Trabzuni D, Guerreiro RJ, Orrell RW, Neal J, Murray A, Pearson J, Jansen IE, Sondervan D, Seelaar H, Blake D, Young K, Halliwell N, Callister JB, Toulson G, Richardson A, Gerhard A, Snowden J, Mann D, Neary D, Nalls MA, Peuralinna T, Jansson L, Isoviita VM, Kaivorinne AL, Hölttä-Vuori M, Ikonen E, Sulkava R, Benatar M, Wuu J, Chiò A, Restagno G, Borghero G, Sabatelli M; ITALSGEN Consortium, Heckerman D, Rogaeva E, Zinman L, Rothstein JD, Sendtner M, Drepper C, Eichler EE, Alkan C, Abdullaev Z, Pack SD, Dutra A, Pak E, Hardy J, Singleton A, Williams NM, Heutink P, Pickering-Brown S, Morris HR, Tienari PJ, Traynor BJ. **A hexanucleotide repeat expansion in C9ORF72 is the cause of chromosome 9p21-linked ALS-FTD.** *Neuron*. 2011 Oct 20;72(2):257-68.

Roselli F, Caroni P. **Modeling neuronal vulnerability in ALS.** *Neuron*. 2014 Aug 20;83(4):758-60.

Rosen DR, Siddique T, Patterson D, Figlewicz DA, Sapp P, Hentati A, Donaldson D, Goto J, O'Regan JP, Deng HX, Rahmani Z, Krizus A, McKenna-Yasek D, Cayabyab A, Gastin SM, Berger R, Tanzi RE, Halperin JJ, Herzfeldt B, Van den Bergh R, Hung WY, Bird T, Deng G, Mulder DW, Smyth C, Laing NG, Soriano E, Pericak-vance MA, Haines J, Rouleau GA, Gusella JS, Horvitz HR and Brown RH. **Mutations in Cu/Zn superoxide dismutase gene are associated with familial amyotrophic lateral sclerosis.** *Nature*. 1993 Mar 4;362(6415):59-62.

Rothstein JD, Martin LJ, Kuncl RW**. Decreased glutamate transport by the brain and spinal cord in amyotrophic lateral sclerosis.** *N Engl J Med*. 1992 May 28;326(22):1464-8.

Rotunno MS, Bosco DA. **An emerging role for misfolded wild-type SOD1 in sporadic ALS pathogenesis.** *Front Cell Neurosci*. 2013 Dec 16;7:253.

Rotunno MS, Auclair JR, Maniatis S, Shaffer SA, Agar J, Bosco DA. **Identification of a misfolded region in Superoxide Dismutase 1 that is exposed in Amyotrophic Lateral Sclerosis.** *J Biol Chem*. 2014 Aug 27. pii: jbc.M114.581801.

Saint-Amant L, Drapeau P. **Motoneuron activity patterns related to the earliest behavior of the zebrafish embryo.** *J Neurosci*. 2000 Jun 1;20(11):3964-72.

Saint-Amant L, Drapeau P. **Synchronization of an embryonic network of identified spinal interneurons solely by electrical coupling.** *Neuron*. 2001 Sep 27;31(6):1035-46.

Sakowski SA, Lunn JS, Busta AS, Oh SS, Zamora-Berridi G, Palmer M, Rosenberg AA, Philip SG, Dowling JJ, Feldman EL. **Neuromuscular effects of G93A-SOD1 expression in zebrafish.** *Mol Neurodegener*. 2012 Aug 31;7:44. doi: 10.1186/1750-1326-7-44.

Shaw PJ, Forrest V, Ince PG, Richardson JP, Wastell HJ. **CSF and plasma amino acid levels in motor neuron disease: elevation of CSF glutamate in a subset of patients.** *Neurodegeneration*. 1995 Jun;4(2):209-16.

Schuster JE, Fu R, Siddique T, Heckman CJ. **Effect of prolonged riluzole exposure on cultured motoneurons in a mouse model of ALS.** *J Neurophysiol*. 2012 Jan;107(1):484-92.

Smith BN, Ticozzi N, Fallini C, Gkazi AS, Topp S, Kenna KP, Scotter EL, Kost J, Keagle P, Miller JW, Calini D, Vance C, Danielson EW, Troakes C, Tiloca C, Al-Sarraj S, Lewis EA, King A, Colombrita C, Pensato V, Castellotti B, de Belleroche J, Baas F, Asbroek ALMA, Sapp PC, McKenna-Yasek D, McLaughlin RL, Polak M, Asress S, Esteban-Perez J, Munoz-Blanco JL, Simpson M, SLAGEN Consortium, van Rheenen W, Diekstra FP, Lauria G, Duga S, Corti S, Cereda C, Corrado L, Soraru` G, Morrison KE, Williams KL, Nicholson GA, Blair IP, Dion PA, Leblond CS, Rouleau GA, Hardiman O, Veldink JH, van den Berg LH, Al-Chalabi A, Pall H, Shaw PJ, Turner MR, Talbot K, Taroni F, Garcıa-Redondo A, Wu Z, Glass JD, Gellera C, Ratti A, Brown RH Jr., Silani V, Shaw CE, Landers JE. **Exome-wide Rare Variant Analysis Identifies TUBA4A Mutations Associated with Familial ALS.** *Neuron*. 2014 Oct 84;2(22):324-331.

Therrien M, Parker JA. **Worming forward: amyotrophic lateral sclerosis toxicity mechanisms and genetic interactions in Caenorhabditis elegans**. *Front Genet*. 2014 Apr 17;5:85.

Thielsen KD, Moser JM, Schmitt-John T, Jensen MS, Jensen K, Holm MM. **The Wobbler mouse model of amyotrophic lateral sclerosis (ALS) displays hippocampal hyperexcitability, and reduced number of interneurons, but no presynaptic vesicle release impairments.** *PLoS One*. 2013 Dec 11;8(12):e82767.

Tong H, McDearmid JR. **Pacemaker and plateau potentials shape output of a developing locomotor network.** *Curr Biol*. 2012 Dec 18;22(24):2285-93.

Tsutsui H, Higashijima S, Miyawaki A, Okamura Y**. Visualizing voltage dynamics in zebrafish heart.** *J Physiol*. 2010 Jun 15;588(Pt 12):2017-21.

Tsutsui H, Karasawa S, Okamura Y, Miyawaki A. **Improving membrane voltage measurements using FRET with new fluorescent proteins.** *Nat Methods*. 2008 Aug;5(8):683-5.

Turner MR, Cagnin A, Turkheimer FE, Miller CC, Shaw CE, Brooks DJ, Leigh PN, Banati RB. **Evidence of widespread cerebral microglial activation in amyotrophic lateral sclerosis: an [11C](R)-PK11195 positron emission tomography study**. *Neurobiol Dis*. 2004 Apr;15(3):601-9.

Turner BJ, Lopes EC, Cheema SS. **Neuromuscular accumulation of mutant superoxide dismutase 1 aggregates in a transgenic mouse model of familial amyotrophic lateral sclerosis.** *Neurosci Lett*. 2003;350:132–136.

Turner BJ, Talbot K. **Transgenics, toxicity and therapeutics in rodent models of mutant SOD1-mediated familial ALS.** *Prog Neurobiol*. 2008 May;85(1):94-134.

Urbani A, Belluzzi O. **Riluzole inhibits the persistent sodium current in mammalian CNS neurons.** *Eur J Neurosci*. 2000 Oct;12(10):3567-74.

Valentine JS, Doucette PA, Zittin Potter S. **Copper-zinc superoxide dismutase and amyotrophic lateral sclerosis.** *Annu Rev Biochem*. 2005;74:563-93.

Van Damme P, Braeken D, Callewaert G, Robberecht W, Van Den Bosch L. **GluR2 deficiency accelerates motor neuron degeneration in a mouse model of amyotrophic lateral sclerosis.** *J Neuropathol Exp Neurol*. 2005 Jul;64(7):605-12.

Van Zundert B, Izaurieta P, Fritz E, Alvarez FJ. **Early pathogenesis in the adult-onset neurodegenerative disease amyotrophic lateral sclerosis.** *J Cell Biochem*. 2012 Nov;113(11):3301-12.

Van Zundert B, Peuscher MH, Hynyen M, Chen A, Neve RL, Brown RH Jr, Constantine-Paton M, Bellingham MC. **Neonatal neuronal circuitry shows hyperexcitable disturbance in a mouse model of the adult-onset neurodegenerative disease amyotrophic lateral sclerosis.** J Neurosci. 2008; 28: 10864-10874.

Vargas MR, Johnson JA. **Astrogliosis in amyotrophic lateral sclerosis: role and therapeutic potential of astrocytes**. *Neurotherapeutics*. 2010 Oct;7(4):471-81.

Vehviläinen P, Koistinaho J, Gundars G. **Mechanisms of mutant SOD1 induced mitochondrial toxicity in amyotrophic lateral sclerosis.** *Front Cell Neurosci*. 2014 May 9;8:126.

Vinsant S, Mansfield C, Jimenez-Moreno R, Del Gaizo Moore V, Yoshikawa M, Hampton TG, Prevette D, Caress J, Oppenheim RW, Milligan C. **Characterization of early pathogenesis in the SOD1(G93A) mouse model of ALS: part I, background and methods.** *Brain Behav*. 2013 Jul;3(4):335-50. (a)

Vinsant S, Mansfield C, Jimenez-Moreno R, Del Gaizo Moore V, Yoshikawa M, Hampton TG, Prevette D, Caress J, Oppenheim RW, Milligan C. **Characterization of early pathogenesis in the SOD1(G93A) mouse model of ALS: part II, results and discussion.** *Brain Behav*. 2013 Jul;3(4):431-57. (b)

Vucic S, Cheah BC, Kiernan MC. **Defining the mechanisms that underlie cortical hyperexcitability in amyotrophic lateral sclerosis.** *Exp Neurol*. 2009 Nov;220(1):177-82.

Vucic S, Lin CS, Cheah BC, Murray J, Menon P, Krishnan AV, Kiernan MC. **Riluzole exerts central and peripheral modulating effects in amyotrophic lateral sclerosis.** Brain. 2013 May;136(Pt 5):1361-70.

Vucic S, Nicholson GA, Kiernan MC. **Cortical hyperexcitability may precede the onset of familial amyotrophic lateral sclerosis.** Brain. 2008 Jun;131(Pt 6):1540-50.

Vucic S, Rothstein JD, Kiernan MC. **Advances in treating amyotrophic lateral sclerosis: insights from pathophysiological studies.** *Trends Neurosci*. 2014 Aug;37(8):433-42.

Vucic S, Ziemann U, Eisen A, Hallett M, Kiernan MC. **Transcranial magnetic stimulation and amyotrophic lateral sclerosis: pathophysiological insights.** *J Neurol Neurosurg Psychiatry*. 2013 Oct;84(10):1161-70. (b)

Wainger BJ, Kiskinis E, Mellin C, Wiskow O, Han SS, Sandoe J, Perez NP, Williams LA, Lee S, Boulting G, Berry JD, Brown RH Jr, Cudkowicz ME, Bean BP, Eggan K, Woolf CJ. **Intrinsic membrane hyperexcitability of amyotrophic lateral sclerosis patient-derived motor neurons.** *Cell Rep*. 2014 Apr 10;7(1):1-11.

Wang J, Farr GW, Hall DH, Li F, Furtak K, Dreier L, Horwich AL. **An ALS-linked mutant SOD1 produces a locomotor defect associated with aggregation and synaptic dysfunction when expressed in neurons of Caenorhabditis elegans.** PLoS Genet. 2009 Jan;5(1):e1000350.

Wang L, Gutmann DH, Roos RP. **Astrocyte loss of mutant SOD1 delays ALS disease onset and progression in G85R transgenic mice.** *Hum Mol Genet*. 2011 Jan 15;20(2):286-93.

Watson MR, Lagow RD, Xu K, Zhang B, Bonini NM. **A drosophila model for amyotrophic lateral sclerosis reveals motor neuron damage by human SOD1.** *J Biol Chem.* 2008 Sep 5;283(36):24972-81.

Westerfield, M. **The zebrafish book. A guide for the laboratory use of zebrafish (Danio rerio)**. 4th ed., Univ. of Oregon Press, Eugene. 2000.

Williams TL, Day NC, Ince PG, Kamboj RK, Shaw PJ. **Calcium-permeable alpha-amino-3-hydroxy-5-methyl-4-isoxazole propionic acid receptors: a molecular determinant of selective vulnerability in amyotrophic lateral sclerosis.** *Ann Neurol*. 1997 Aug;42(2):200-7.

Wong M, Martin LJ. **Skeletal muscle-restricted expression of human SOD1 causes motor neuron degeneration in transgenic mice.** *Hum Mol Genet*. 2010 Jun

1;19(11):2284-302.

Yamanaka K, Chun SJ, Boillee S, Fujimori-Tonou N, Yamashita H, Gutmann DH, Takahashi R, Misawa H, Cleveland DW. **Astrocytes as determinants of disease progression in inherited amyotrophic lateral sclerosis.** *Nat Neurosci*. 2008 Mar;11(3):251-3.

Zamani M, Elias M, Tousley ME, Amador Kane S. **Tracking Multiple Objects Using ImageJ with tracking plugins**. 2011.

PUBLICATIONS

Benedetti L*, Sogne E*, Rodighiero S, Marchesi D, Milani P, Francolini M. **Customized patterned substrates for highly versatile correlative light-scanning electron microscopy.** Sci Rep. 2014 Nov 13. 4:7033-doi:10.1038/srep07033

Bazzini C, Benedetti L, Civello D, Zanoni C, Rossetti V, Marchesi D, Garavaglia ML, Paulmichl M, Francolini M, Meyer G, Rodighiero S. **ICln: A New Regulator of Non-Erythroid 4.1R Localisation and Function.** *PLoS One.* 2014 Oct 8;9(10):e108826. doi: 10.1371/journal.pone.0108826. eCollection 2014.

Recordati C, Basta SM, Benedetti L, Baldin F, Capillo M, Scanziani E, Gobbi A. **Pathologic and Environmental Studies Provide New Pathogenetic Insights Into Ringtail of Laboratory Mice.** *Vet Pathol.* 2014 Nov 5. pii: 0300985814556191

ACKNOWLEDGEMENTS

I would like to thank Prof. Alberto Panerai, who, during these years, coordinated with passion the Ph.D. School in Pharmacological Sciences.

I would like to acknowledge Dr. Christine E. Beattie who gave us the wild-type and mutant Sod1 zebrafish transgenic lines and Dr. Hideaki Tsutsui who gently provided us the voltage biosensor Mermaid that demonstrated an extremely powerful tool for the study of neuronal electrical properties.

Special thanks are due to Dr. Maura Francolini and Dr. Simona Rodighiero who supervised me and allowed me to grow as a scientist and, above all, gave me the opportunity to deepen from several point of view one of my greatest passion: microscopy!

I am grateful to Dr. Luca del Giacco, Anna and Laura who introduced me in the zebrafish world and taught me a bit of molecular biology like no other could do! I would like to thank them for helping me carrying out part of this work not only with practical experiments but also with constructive discussions and several Nespresso's coffees.

I would like to thank Dario Parazzoli and Max Garrè who gave me the opportunity to use the two-photon excitation microscope and thought me how to detect myosin SHG signal.

I sincerely thank my colleagues, or better dear friends, especially Elena, Elisa, Marcella, Elsa, Mila, Marianna, Marta and Rocco who sustained me every day starting from the morning coffee, to the gossip at lunch and till the evening Negroni.

Last but most important, I heartily thank my dear family, my beloved mate and my far but closest friends Ile and Vale who always supported me during these years.